CHARACTERIZATION OF LASER CUTTING ON STAINLESS STEEL (AISI-304) AND FUNCTIONALLY GRADED MATERIAL (NICKEL -STAINLESS STEEL)

A thesis submitted towards partial fulfillment of the requirements for the degree of

Master of Technology in Laser Technology

Course affiliated to Faculty of Engineering and Technology and
offered by Faculty Council of Interdisciplinary Studies, Law and Management,
Jadavpur University

submitted by

SUBHA NATH
Examination Roll No. :M4LST19005
Registration No.:141052 of 2017 – 2018

Under the guidance of

Assoc. Prof. Dr. Amit Karmakar
Department of Mechanical Engineering
Jadavpur University, Kolkata - 700032

School of Laser Science and Engineering

Faculty Council of Interdisciplinary Studies, Law and Management

Jadavpur University

Kolkata -700032

India

2019

M. Tech in Laser Science & Technology
Course affiliated to
Faculty of Engineering and Technology
and offered by
Faculty Council of Interdisciplinary Studies, Law and Management
Jadavpur University
Kolkata, India

CERTIFICATE OF RECOMMENDATION

THIS IS CERTIFIED THAT THE THESIS ENTITLED " **CHARACTERIZATION OF LASER CUTTING ON STAINLESS STEEL (AISI-304) AND FUNCTIONALLY GRADED MATERIAL (NICKEL -STAINLESS STEEL)**" IS A BONAFIDE WORK CARRIED OUT BY **SUBHA NATH** UNDER MY SUPERVISION AND GUIDANCE FOR PARTIAL FULFILMENT OF THE REQUIREMENT FOR POST GRADUATE DEGREE OF MASTER OF TECHNOLOGY IN LASER TECHNOLOGY, DURING THE ACADEMIC SESSION 2018-2019.

THESIS SUPERVISOR
Assoc. Prof. Dr. Amit Karmakar
Department of Mechanical Engineering,
Jadavpur University, Kolkata-7000032

Countersigned

SRI. DIPTEN MISRA
Director
School of Laser Science and Engineering
Jadavpur University, Kolkata-700 032

DEAN
Faculty Council of Interdisciplinary Studies, Law and Management
Jadavpur University, Kolkata-700 032

M. Tech in Laser Science & Technology
Course affiliated to
Faculty of Engineering and Technology
and offered by
Faculty of Interdisciplinary Studies, Law and Management
Jadavpur University
Kolkata, India

CERTIFICATE OF APPROVAL **

This foregoing thesis is hereby approved as a creditable study of an engineering subject carried out and presented in a manner satisfactory to warrant its acceptance as a pre-requisite to the degree for which it has been submitted. It is understood that by this approval the undersigned do not necessarily endorse or approve any statement made, opinion expressed or conclusion drawn therein but approve the thesis only for the purpose for which it has been submitted.

COMMITTEE OF FINAL EXAMINATION ----------

FOR EVALUATION OF THESIS

** Only in case the recommendation is concurred

DECLARATION OF ORIGINALITY AND COMPLIANCE OF ACADEMIC ETHICS

The author, hereby declares that this thesis contains original research work by the undersigned candidate, as part of his **Master of Technology in Laser Technology** studies during academic session 2018-2019.

All information in this document has been obtained and presented in accordance with academic rules and ethical conduct.

The author also declares that as required by this rules and conduct, the author has fully cited and referred all material and results that are not original to this work.

NAME:**SUBHA NATH**

EXAMINATION ROLL NO..**: M4LST19005**

THESIS TITLE: **CHARACTERIZATION OF LASER CUTTING ON STAINLESS STEEL (AISI-304) AND FUNCTIONALLY GRADED MATERIAL (NICKEL -STAINLESS STEEL)**

SIGNATURE: DATE:

ACKNOWLEDGEMENT

I express my sincere gratitude to my supervisor **Assoc. Prof. Dr. Amit Karmakar** for his invaluable guidance, whole-hearted support and encouragement for accomplishing the present investigation. His dynamism, fantastic stamina and day-to-day monitoring every minute detail were a constant source of inspiration to me.

I express my great depth of gratitude to **Dr. Paramasivan Kalvettukaran, Aparna Sudha Kiran, Dr. Apurba Das, Mohsina Hossain Nobony and Lumina Rashid** for their inspiration and encouragement and helping me through the research work.

I would also like to express my deep sense of thankfulness to **Sri. Dipten Misra** providing me necessary atmosphere to work on.

I record my acknowledgement to **School of Laser Science and Engineering** for giving me the opportunity to pursue my research work.

Lastly but obviously not the least I would like to pay my special admiration thanks to my parents and brother for their constant support, love and faith.

My eternal gratitude goes to god.

.

SUBHA NATH

Examination Roll No.:M4LST19005

Registration No.:141052 of 2017 – 2018

Contents

b) Summary of laser cutting on FGM

6.2. Future scope

References

Chapter 1: General Introduction

1.1. Introduction

The word laser stands for light amplification by stimulated emission of radiation. The laser technology field has hugely expanded science the laser was first invented in early of 1960.After that laser is found in various types of applications like including active imaging, active remote sensing, optical communication, power beaming and high energy weapons.

Monochromatic, directional and coherent properties are the unique characteristics which open a golden chapter of non conventional technology. Lasers are devices that utilize energy levels between molecules for the generation of coherent radiation. That radiation can be used from bloodless surgery to applying destructive military power.

In the last twenty to twenty-five years science the first appearance of lasers have become widespread and most common device for commercial applications. The importance and excitement of laser and its applications still be hardly overestimated.

LASER (Light Amplification by Stimulated Emission of Radiation) is a monochromatic, directional, coherent light beam which plays great role in manufacturing industry science 1960.Laser system consists of a laser cavity which is excited by flash light and produces stimulated emission known as laser. The laser is guided by mirror and focused by a convex lens. The focused beam can be considered as a heat source. The heat flow increases the temperature continuously of that spot, due to that phase change takes place. The phase change material (either liquid or vapour) is removed by assist gas and machining takes place [1].

The functional graded material (FGM) is a unique type of composite material which is widely used in engineering applications as it is free from de-bonding and de-lamination effects unlike other composite materials [2]. Because of wide use of such material, different machining techniques of such material are a promising area of research now a day. Among different machining techniques, laser cutting finds prime significance in FGMs for better accuracy[3].

On the other hand, Stainless steel-304 is austenitic alloy consists of carbon(0.055%), phosphorus(0.029%), manganese (1%), silicon(0.6%), sulphur (0.005%), chromium(18.28%) and nickel (8.48%)[4].Hence, heating and rapid cooling associated with laser cutting of stainless steel AISI-304 initiates grain refinement, phosphate, carbide, sulphide formation, known as Heat affected zone (HAZ)[5-7]. It is an undesirable phenomenon which has some backlogs. Also, during laser cutting considering the temperature gradient, large thermal stress is develop which may exceed the yield point of the material and produce crack or fracture.

1.2.Different types machining processes

There are several types of machining processes are given Fig.1.1below [8].

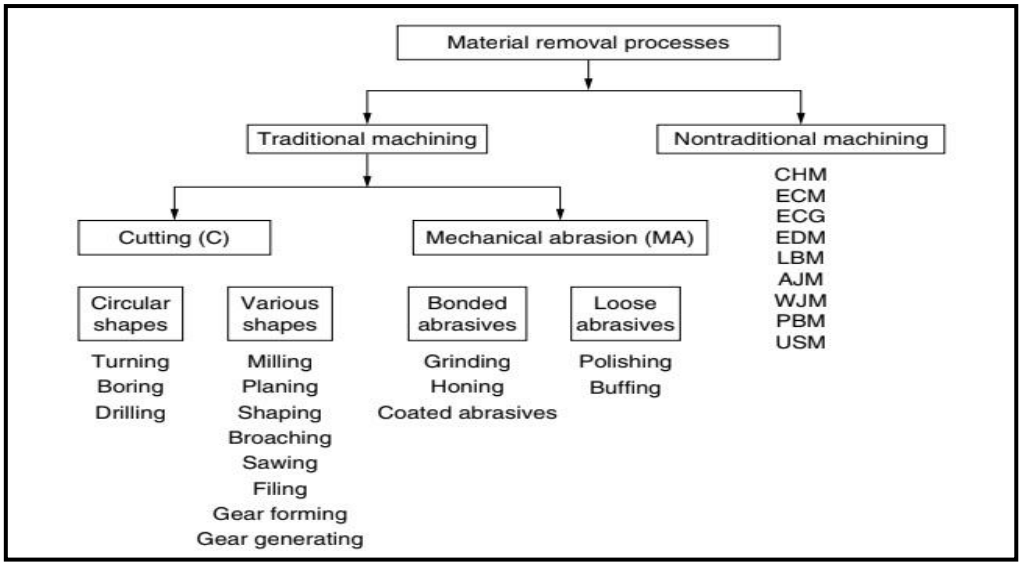

Fig. 1.1: Different types of material removal process

1.2.1. Conventional machining processes

Conventional machining process is also known as traditional machining, in which the cutting tool remove the material by penetrating in it. In this process the cutting tool is harder than the machining tool. There is a relative motion between the tool and the workpiece and the motion is provided by the prime mover. The relative motion provides desired shape of the material by giving certain depth. In this regard, shaping and milling generate flat surfaces; turning produces cylindrical parts, while drilling produces holes of different radius. There is a specific geometry of specific machine tool and specific number of cutting edges on it.

The cutting operation produces allowances to chips which can easily visible with naked eyes[8]. Different types of conventional machining processes are given in Fig.1.2 [9-12].

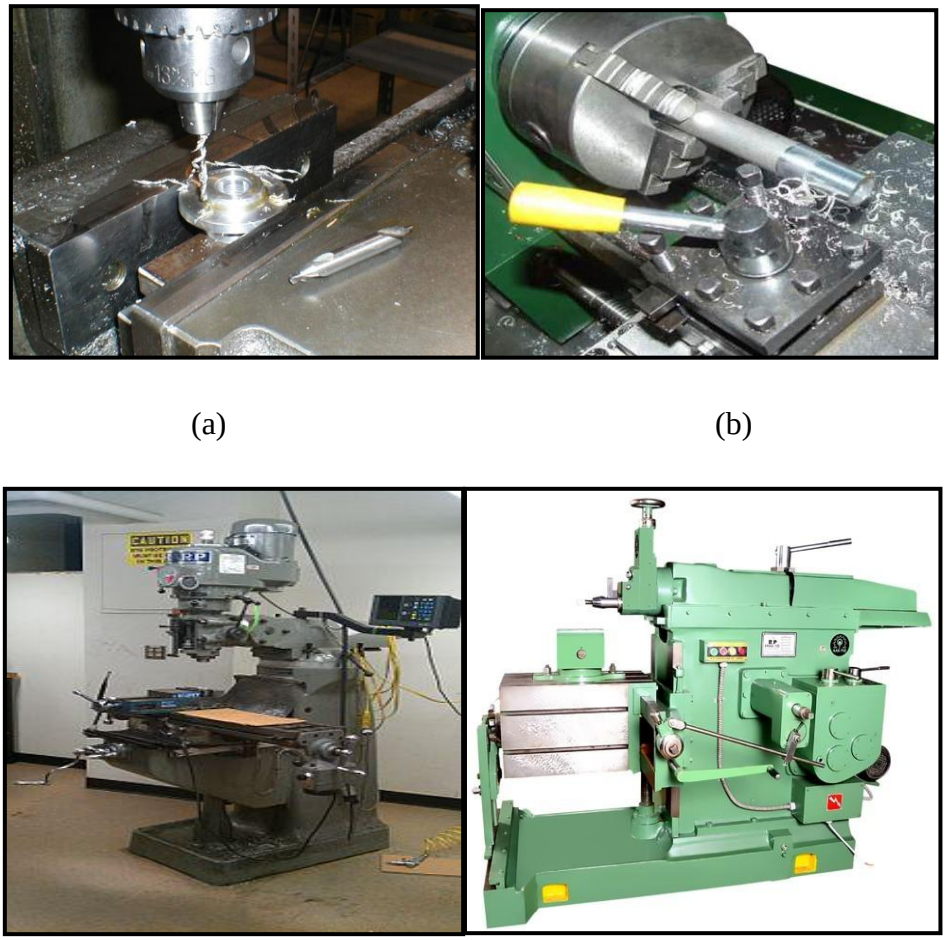

(a) (b)

(c) (d)

Fig. 1.2: Different types of conventional machining process

1.2.2. Non-conventional machining processes

The greatly improved thermal, chemical, and mechanical properties of the new engineering materials made it impossible to machine them using the traditional machining processes of cutting and abrasion. In the traditional process tool material is harder than the work piece material. It is very difficult to machine highly hardness material (ceramic) or making complex shape or low rigidity structure with the help of traditional machining process. Non-

conventional machining process gives huge success in that type of machining process which is applicable in automobile and aircraft industry [8].

There are some non- conventional machining processes are described below.

1.2.2.1. Water jet machining

Water jet machining, also known as water jet cutting is a non-conventional machining process. It was introduced in early 70's.With or without abrasive highly pressurised water is hit on the specimen and removes some material and does machining operation. The speed of the water jet is supersonic (generally almost three times of sound) and with highly kinetic energy it penetrates the specimen. Though there are several types of water jet machining process but the basic methodology remains same in all the processing. Here water is pumped at a sufficiently high pressure (approximately 200 to 400 MPa.) using intensifier technology. An intensifier works on the simple principle of pressure amplification using hydraulic cylinders of different cross sections. At such pressure when water is issued through a suitable orifice generally of 0.2 to 0.4 mm diameter, the potential energy of water is directly converted into kinetic energy, yielding a high velocity jet (nearly 1000 m/s). Such high velocity water jet can machine thin sheets or foils of leather, textile, frozen food, aluminium etc.

There are several types of water jet machining as enumerated below:

a) According to the process: stabilizer WJM; Pure WJM; AWJM entrained (three phase) abrasive, water and air and AWJM suspended (two phase) abrasive and water.
b) According to the pumping: Indirect pumping; Direct pumping and Bypass pumping.

There are wide applications of water jet machining in technology. Mainly this mechanism is used in Cleaning, Paint removal, Turning, Cutting soft material and Drilling etc.[13]The process of water jet machining is shown in Fig.1.3 below [14] .

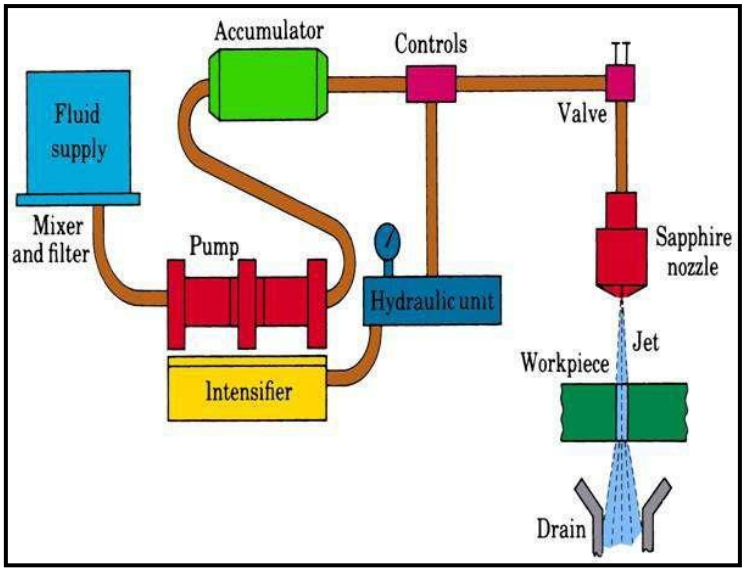

Fig. 1.3: Abrasive water jet machining process

There are many advantages of water jet machining as follow:

a) The water jet cutter does not create any harmful waste and with a small kerf, it also facilitates the recyclability of scrap metal.
b) When compared to other cutting process, the water jet cutter able to handle all material or product that a traditional cutter can. Traditional tough materials such as bullet-proof glass, stone, metals or even materials with reflective or uneven surfaces can all be cut through with water jet.
c) Water cutters do no overheat the areas adjacent to the cutting portion; therefore these pieces stay uncompromised and intact.
d) Water jet cutter is capable of achieving very intricate cuts or 3-D shapes and 0.13 mm accuracy.

There are some disadvantages of water jet machining as given below:

a) While the water jet cutter can cut most of the same materials, very often the cutting takes longer than a traditional cutter. More time cutting means less output.
b) Low quality water jet orifices have a tendency to breakdown and disrupt cutting, resulting in lost time and productivity.

c) The thicker a material the further the stream is away from the nozzle at its point of impact. A less consistent impact from water jet changes the cutting accuracy from top to bottom. Often, the jet can spread and make more of a diagonal cut than a straight up and down cut.

d) In the beginning, finding and implementing the additional abrasive materials, like granite, to increase the efficacy of the cutter can by very expensive compared to a simple plasma cutter [15].

1.2.2.2.Ultrasonic machining

The ultrasonic machining is a nonconventional where abrasive contained in slurry is driven against the work by oscillating at high frequency (15 to 25 kHz) and low amplitude (25 to 100 microns).In this process there is a vibrating tool vibrates and applies a fluctuating load over the workpiece. Hard abrasive particles are present in the machining zone (between tool and the workpiece) and the abrasive particles, as they indent, the work material, would remove the same, particularly if the work material is brittle, due to crack initiation, propagation and brittle fracture of the material[16].The process of Ultrasonic machining is shown below in Fig. 1.4 [17].

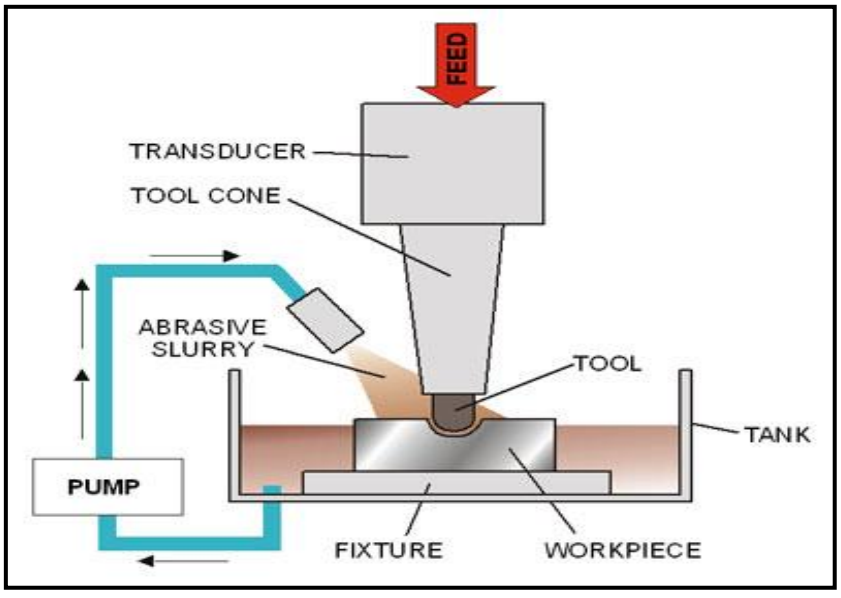

Fig. 1.4: Ultrasonic machining process

1.2.2.3. Laser beam machining

In the laser machining process laser beam works as a heat source which heated part of a material. That part material reaches above the melting or the vaporization point and phase change takes place. The molten or vaporized material is removed by assist gas.

1.3. Laser beam cutting

Laser beam cutting is one the accurate and cost-effective approach in manufacturing. Precision cutting, easy automation, less deformation and high quality are the golden sides of this process to make large application in manufacturing industry. In this process up to thickness 25 mm sheet can cut effectively with very less heat affected zone (HAZ). Laser cutting works on the principle of localised heating (due to high intense light) and changes the phase of the localised material. It controlled by a programmed cutting path where the beam passes through. There are several assist gases which play important role in cutting process. Generally, two types of assist gases are used in Laser cutting process. On one hand for the sake of high precision, minimum HAZ and without oxidisation cutting nitrogen gas (N_2) or inert gas (like Argon, Neon etc) used to utilized as shielding gas (protect from reaction with air). On the other hand for high production and oxidisation cutting oxygen (O_2) or air is used. The depth of cut, width of cut, striation, doss formation etc. effects are dependent on the parameters of the laser beam. Generally laser beam power, scanning speed beam diameter and material properties are the parameter which plays main role in laser cutting.

1.3.1. Principles of laser beam machining

Basically, in this process LASER (Light Amplification Stimulated Emission of Radiation) is a high intense coherent light (photon energy) strikes the surface of the localised area of the specimen and increases the temperature of that area. Continuous heat flow increases the temperature of the top surface and phase change of the material occurs (melt or vaporized).Generally, nanosecond or femtosecond laser is used for the machining process to make the absorb energy more than conductive energy. The phase change material produces ‘Keyhole’ which quickly deepens the depth and the width of cut (due to increase the

absorbing energy due to multiple reflections. The molten or vaporised gas is removed by the assist gas. The process of laser beam machining process is shown in Fig.1.5 below [18].

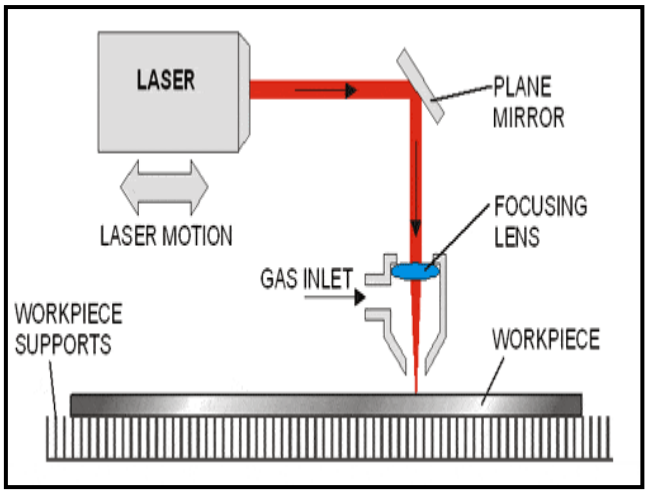

Fig. 1.5: Laser beam machining process

a) Sublimation cutting:

In the presence of high power (generally 10^6 W/cm^2 for metal) the material temperature reaches above the evaporation point. Hence the material of that area is directly converted into the vapour without occurring molten condition. This laser cutting process is known as Sublimation cutting. The vapour is removed by the assist gas. This process is highly applicable for thin sheet and also for some non metal like wood, carbon and some plastics. Assuming one dimensional heat flow with total vaporisation (neglecting the heat losses e.g. through conduction, radiation) the penetration depth follows:

$$D_P = \frac{\eta P}{\rho V_0 D_B (L + C_P (T - T_a))} \tag{1.1}$$

The time at which the beam with transverse velocity of V_0 travels a distance equal to its diameter D_B, follows:

$$t = \frac{D_B}{V_0} \tag{1.2}$$

Assuming instant penetration through the material thickness, the volume removed per second per unit area equals the penetration velocity:

$$V = \frac{D_P V_0}{D_B} \tag{1.3}$$

Hence,

$$V = \frac{\eta P}{\rho D_B^2 (L + C_P (T - T_a))} \tag{1.4}$$

Where D_p (mm) is the penetration depth, η is the absorptivity of the material, P (W) is the laser beam power, D_B (mm) is the focused beam diameter, V_0(mm/s) is the transverse velocity of the beam, V (mm/s) is the penetration velocity, t(s) is the time elapsed to travel a distance d (mm), ρ(kg/m^3) is the work piece density, L (J/kg)is the latent heat of fusion and vaporisation, C_P (J/(kg.K)) is the heat capacity of work piece, T is the vaporisation temperature (K) and T_a (K) is the initial temperature of material.

b) Fusion cutting

In the fusion the material cannot reached above the evaporation point due to lower power of the beam. Hence the material is melted and the molten material is removed by the assist gas. It is highly applicable for thick plate and the high evaporating pointed material.

c) Oxygen assisted laser cutting

With the help of oxygen (or air) in high temperature material produces exothermic reaction which helps to melt more material. Hence high penetration and quick process is achieved in this process. This process is very useful of cutting thick plate or materials which has high melting point.

d) Scribing

In this process a slot or series of blind holes create on the surface of the specimen enough to raise the stress locally so that the material can be easily fractured along the desired line.

e) Controlled fracture cutting

In this process a low power beam is used to propagate a crack (at speeds up to 1 m/s) by local thermal stresses. This process is applicable for cutting brittle materials. The main associated problem is control of the cut path at the edges of the specimen.

f) Photo-chemical cutting (cold cutting)

In this process laser beam with high photon energy (UV) is used to break the chemical bonding between the molecules and produces new components. It is especially practical for woods. But the machining rate is lower than the others [19].

1.3.2. Laser beam machining of Stainless Steel

Stainless steel-304 is a corrosion free austenitic steel alloy having high melting temperature (1450°C).Moreover, it contains significant proportion of carbon (0.055%), manganese (1.00%), phosphorus (0.029%), sulphur (0.005%), silicon (0.6%), chromium(18.28%), nickel (8.48%)[4].Hence, heating and rapid cooling associated with laser cutting of stainless steel-304 initiates grain refinement, carbide, sulphide and phosphate formation, known as HAZ [5-7].

There are wide applications of stainless steel of laser cutting due to its superior light absorbing property [20]. No tool loss, narrow fine cut, less heat affected zone (HAZ) and easy to automation properties of laser gives huge advantages of cutting of stainless steel than the traditional cutting process. There are several applications of stainless steel AISI-304 are shown in the Fig. 1.6 below[21].

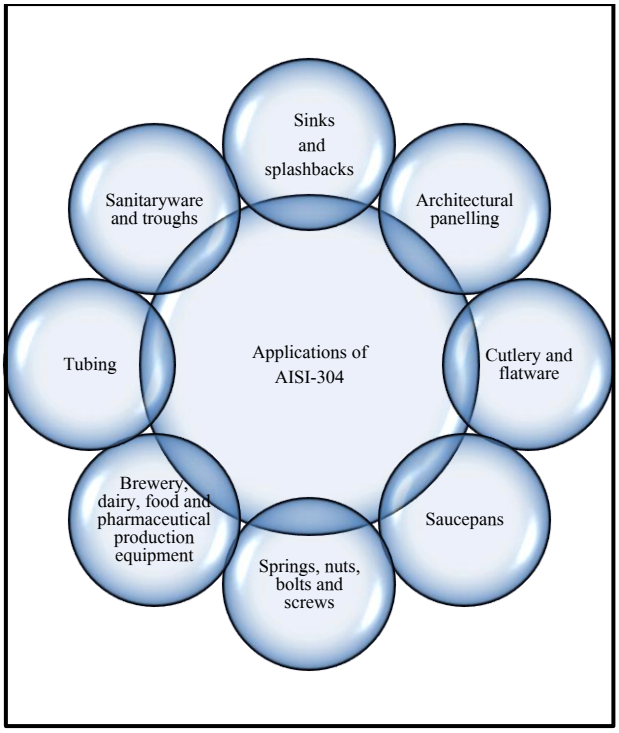

Fig. 1.6: Application of stainless steel AISI-304

In this thesis, a comparative study of laser cutting was performed with the help of experimental and numerical investigations on stainless steel (AISI-304). Dimension of the stainless steel (AISI 304) specimen was modelled as 75mm × 80mm × 0.5 mm (X × Y × Z).The Laser cutting of stainless steel AISI-304 is depicted below in the Fig.1.7 [22].

Fig. 1.7: Laser cutting of stainless steel AISI-304

1.3.3. Laser beam machining of Functional Graded Material(FGM)

The aim of the designing material is to perform a set of specified functions. The concept of the FGM(Functionally graded material) material was developed for changing the sharp interface to the gradually changing interface. Functionally graded material changes its microstructure, composition or porosity across the volume. It is a special type of composite material which is inhomogeneous (microscopically). Moreover, in case of FGM material the properties of the material(chemical, mechanical, magnetic, thermal and electrical) vary throughout the material[23]. The pictorial view of Functionally Graded Material (FGM) is shown in Fig. 1.8.

Fig. 1.8: Functionally graded material (FGM)

Functionally graded material is widely used in various engineering applications for the advantages offered by the properties of materials in combination. The present areas of applications include aerospace, automobile, biomedical, defense, electrical or electronic,

energy, marine opto-electronics, and thermo-electronics. There are several types of FGM materials and their applications are shown in the Fig. 1.9 below [24].

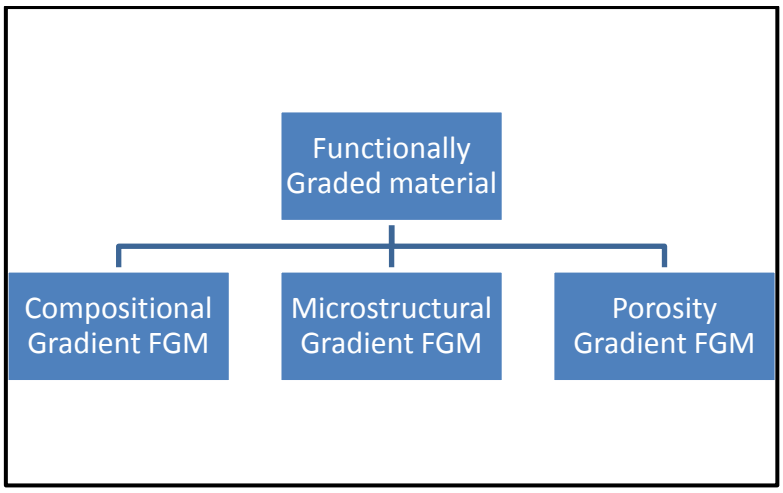

(a)

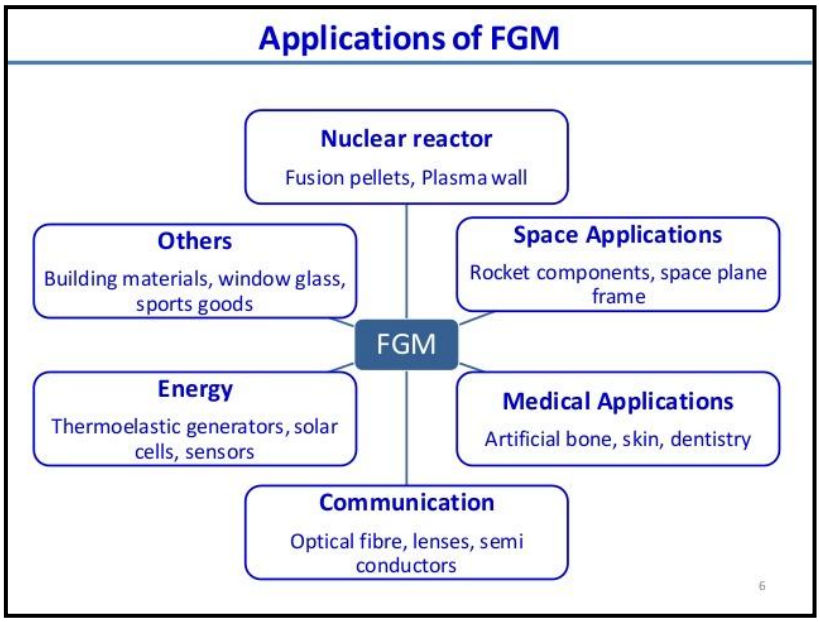

(b)

Fig. 1.9: (a)different types of FGM and (b)Application of Functionally graded material (FGM)

In this thesis also numerical computational analysis of rectangular plate made of stainless steel (AISI 304) - Nickel (Ni) FGM material is considered. Dimension of the work piece is

modelled as 15mm × 25mm × 8 mm. Each layer of FGM material is 1 mm thick and possesses the same material properties using Comsol Multiphysics 5.3a software.

Chapter 2: Literature Review and Objectives of Present Study

2.1. Literature Review of Laser Cutting on Stainless Steel and Functionally Graded Material (FGM)

Wandera et al.[25] presented experimental analysis of laser cutting on stainless steel (AISI-304). The analysis is done by fibre laser, disc laser and CO_2.In this study kerf width, depth of cut, depth of cut and surface roughness is measured at different laser types and different laser parameters such like laser power and scanning aped.

Wandera and Kujanpaa[26] analyzed the characterization of the melt removal rate in laser cutting of thick-section stainless steel. In this study a experimental analysis is done by varying effective parameters like laser power, cutting speed, nozzle diameter and gas pressure.A fiber laser (IPG YLR 5000) of maximum capacity of 5 kW is used in this investigation. Results are found that The assist gas pressure, nozzle diameter, and focal point position are found to significantly affect the efficiency of melt removal from the cut kerf. .

Stelzer et al.[27] presented experimental investigations on fusion cutting stainless steel with fiber and CO_2 laser beams. In this study, the cutting capabilities of a fiber and a CO2 laser beam with similar Rayleigh length have been compared as a function of material thickness with respect to reachable maximum cutting speed, cut edge surface roughness and cut kerf geometry.It is observed that cut kerfs are nearly identical in size but differ qualitatively in shape for both laser types.

Wandera et al. [28] observed Inert gas cutting of thick-section stainless steel and medium-section aluminium using a high power fiber laser. The laser cutting of 10 mm stainless steel plate and 4mm aluminium sheet with a high power fiber laser has been investigated in this paper. The maximum cutting speeds at different laser power levels were determined. The effects of focus position and assist-gas pressure on the cut surface roughness were also examined.

Nyon et al.[29] presented the experimental laser cutting process of continuous laser as well as simulation of laser cutting process in ANSYS. There is a comparison between simulation and experimental results of cutting width of Inconel 718.Also, laser cutting was simulated at continuous wave (CW) and the effects of laser power and cutting speed on kerf width were investigated. the simulation results agreed well with the experimental results.

Sifullah et al.[30] compared experimental and simulation results on laser fusion cutting of stainless steel AISI-304.The simulation was performed on ANSYS software and continuous laser operation was done in this study. The present study revealed that maximum temperature was developed close to the heat source and the width of HAZ increases with increase of laser power and decrease with increase of cutting speed. Cracks and dross were found along the cutting edge, which are more noticeable at the middle of the specimen as maximum stress concentration as shown by FE analysis.

Fu et al.[31] made experimental analysis on fiber laser cutting of Nitinol and the kerf geometry, roughness, topography, microstructure, and hardness analysis was done to understand the nature of Heat Affected Zone (HAZ). A good correlation was found between predicted kerf geometry and the experimental data. Moreover, the effects of cutting speed, pulse power, and pulse width on kerf profile, temperature, and heat affected zone (HAZ) were investigated.

Kardas et al.[32] performed laser cutting of rectangular geometry in 2024 aluminum under high pressure nitrogen assisting gas. Temperature and thermal stress fields are predicted in the cutting region using ABAQUS finite element code. It is found von Mises stress attains significantly high values in the close region of the corners of the cut edges and mid thickness of the cutting section along the rectangular geometry. The laser cutting section was free from large asperities like cracks and sideways burnings. It was also observed that local dross attachment at the kerf exit.

Wang [33] performed by using CO_2 laser an experimental cutting analysis is done on a metallic coated sheet steels. Relationships among the cutting speed, laser power and specimen thickness, from which a recommendation was made for the selection of optimum cutting parameters for processing GALVABOND material from statistical analysis. It has been revealed that although high laser power permits high cutting speed to be used for good quality cuts, this trend does not apply when the laser power was above a threshold value in which case no class III cut was produced .The combinations of input process parameters for

class III cuts with minimum HAZ and dross was graphically presented together with the recommended optimum process parameters for practical applications.

FGM structures have been recently used in turbo machinery blades for their associated behavior during service especially in the aerospace, aviation, marine and automotive industries. A good amount of research knowledge has been made available in numerous monogram, review and different scientific journals. The literature related to the analysis, design and modeling of FGM plate and shells covers a wide area of research. The shallow shell has a lesser thickness compared to its other dimensions and in which deformations are not large compared to thickness. Shell structures of twisted geometry have immense applications in the area of mechanical structural components. The literatures related to design, modeling, analyses and construction of shell structures cover a broad area of research, especially in the context of the present work. Significant development has taken place in usage of these specialized structures with the introduction of functionally graded materials. Accordingly, the main emphasis is given with reference to the dynamics of FGM structures in respect of finite element modeling, dynamic response of prêt-wisted rotating FGM plates and shells under low velocity impact.

Extensive applications of shell forms as turbo-machinery blade structures have a long history although plethora of investigations made on the properties of shell structures initiated about hundred years ago. The historical review on the course of shell research and design was presented by Rotter [34] while the principle and techniques of vibration portrayed by Meirovitch [35]. Vibration characteristics of turbo machinery blade profiles are presented by Rao[36]. Isotropic shells was initially used for research later on the focus was given to the composite laminated shell, but at high thermal gradient the de-lamination is major concern for the composite shell. Therefore since the introduction of FGMs from last two decades lot of attention is given on FGMs shells and structures. FGM materials are gaining wide applications in various branches of engineering and technology with a view to make suitable use of potential properties of the available materials in the best possible way. This has been possible through research and development in the area of mechanics of FGMs for the present day modern technologies of special nuclear components, spacecraft structural members, and high temperature thermal barrier coatings, etc. De-bonding or de-lamination are the main problem of advanced fiber reinforced composite laminates where the separation of layers caused by high local inter-laminar stresses reduces the stiffness and structural integrity no longer maintained. FGMs have the potential to eliminate these problems and due to these

advantages FGMs have gained huge importance as an advanced material. The most common FGMs are metal-ceramic constituents, where the ceramic part has good thermal resistance and metallic part has superior structural support. The turbo-machinery blade materials with FGM have all these advantages compare to the composite and conventional material considering both thermal and structural aspect.

Review articles like those by Birmanand Byrd [37], Liew et al.[38], Alijaniand Amabili [39], Jhaet al. [40], Thai and Kim[41], Swaminathanand Naveenkumar[42], Gupta and Talha [43], Liew et al.[44],Swaminathan and Sangeetha[45]covered much of the research done within last two decades while very little attention was given to FGM conical shells prior to that except reported by Zhaoand Liew[46] and Tornabene et al.[47].

2.2. Objectives of the present study

Firstly,the objective of this thesis work is to investigate numerically and experimentally the effects of process parameters: laser power and scanning speed on kerf width, depth of cut, HAZ and thermal stress of stainless steel (AISI-304) having thickness 0.5mm.Gaussian heat source, representing the laser beam, is applied along a straight line path through the middle of the work piece. The work piece is assumed to be symmetric. The model is meshed with non-uniform pattern triangular mesh.

Secondly, laser cutting on Functionally Graded Material (FGM) is carried out verifying with laser cutting of stainless steel(experimental and simulation) to obtain the thermal stress, displacement, kerf width, depth of cut and thermal stress thereby to understand the mechanism of laser cutting process with greater insight. A thermo-mechanical FEM model for sublimation laser cutting on functionally graded material (FGM) was perused by using Gaussian distributed heat flux to predict the kerf width, depth of and stress field. The numerical simulation was performed on FGM using different laser powers and scanning speeds.

Chapter 3: Experimental Setup, Plan and Procedure

3.1. Laser Beam Machining System

The pictorial view of experimental set up for laser cutting (ELECTROX EMS 100) is shown in Fig. 3.1.

Fig. 3.1: Laser cutting setup **(**ELECTROX EMS 100)

Table 3.1: Neodymium-doped Yttrium Orthovanadate (Nd: YVO_4) Laser Specification

ELECTROX EMS 100 Laser Specification	
LASER TYPE	Nd:YVO_4
WAVELENGTH	1064 nm
MAXIMUM POWER	9.28 W
FREQUENCY	0 TO 500 kHz
SCANNING SPEED	0.15 TO 10160 mm/s
BEAM DIAMETER	40 TO 50 µm
PULSE ON TIME	4 ns

Laser Beam Scanner Specifications

The Electrox UV laser cutting system produces cuts at the following specification.

Table 3.2: Laser Beam Scanning Specifications

WRITING SPEED(mm/s)	FROM 0.50 UPTO *10000
POSITIONING RESOLUTION(mm)	**0.005
CHARATER SIZE(mm)	0.5-100

* This value is dependent upto the type of scanning assembly used and the software / firmware version.

** This value is calculated using a 163 mm scanner lens with a maximum field size of 144 mm.

Physical Dimension

Table 3.3: Physical Dimensions Of Laser Cutting Machine

	WEIGHT	DIMENSIONS(H×L×W) mm
LASER ENCLOSURE	16 kg	230 × 1040 × 200
CONTROL UNIT	40 kg	267.4 × 553 × 552.4
CHILLER	8.8 kg	386 × 277 × 203

Facility Requirement - Electrical Power Supply

Table 3.4: Electrical Power Supply

ELECRICAL SUPPLY	2-PHASE AND EARTH, OR PHASE, NEUTRAL AND EARTH
STANDARD VOLTAGES	100-240 Vac.
STANDARD SUPPLY FREQUENCIS	50/60 Hz
SUPPLY RATING	1.0 kVA.

Environmental Requirements

Temperature and Humidity are the factors of environmental condition.

Table 3.5: Environmental Requirements

AMBIENT TEMPERATURE RANGE (OPERATIONAL)	16-35°C
AMBIENT TEMPERATURE RANGE (STORAGE)	5-40°C
HUMIDITY	NON-CONDENSING ON A 15°C SURFACE

Vibration (During Transportation)

Table 3.6: Vibration (During Transportation)

PERMISSIBLE VIBRATIONS	SINUSOIDIAL EXCITATION 10-150 Hz SLIDING FREQUENCY
PERMISSIBLE LOAD	0.75 mm / 5 kg
PERMISSIBLE SHOCKS CONTROL UNIT 10 g / 11 ms	SEMI-SINUSOIDIAL,MAX 10 g/ 11ms SEMI-SINUSOIDIAL, MACX LASER ENCLOSURE

The control unit contains the following electrical modules:

i. Main disconnect switch (Isolator)
ii. Auxiliary power supplies
iii. DSP(laser beam scanner) PCB
iv. CPU PCB
v. USB PCB
vi. I/O PCB (interface PCB)

The laser power supply contains:

i. Diode laser power supply
ii. Q-switch power supply
iii. Gain and wavelength media temperature control systems.

3.1.1.Nd:YVO_4 Laser Machining System

Neodymium-doped yttrium orthovanadate (Nd: YVO_4) is a crystalline material formed by doped neodymium ion to yttrium orthovanadate. It is commonly used as an active laser medium for diode pumped solid-state lasers. It comes as a transparent blue-tinted material. It is bi-fringe; therefore rods made of it are usually rectangular. As in all Neodymium-doped laser crystals, the lasing action of Nd: YVO_4 is due to its content of neodymium ions, which may be excited by visible or infrared light, and under an electronic transition resulting in emission of coherent infrared light at lower frequency, usually at 1064 nm.

3.2. Optical Microscope

Width and depth of laser cutting of stainless steel AISI-304 specimens were measured with optical microscope using 5X magnification.

Fig 3.2: OLYMPUS Microscope BX53

3.2.1.OLYMPUS Microscope

The specification of OLYMPUS microscope is given in the Table 3.7 below.

Table 3.7: OLYMPUS Microscope Specification

BX53 specifications

Microscope frame	Optical system	UIS2 optical system
	Focus	Vertical stage movement: 25 mm stage stroke with coarse adjustment limit stopper, Torque adjustment for coarse adjustment knobs, Stage mounting position variable, High sensitivity fine focusing knob (minimum adjustment gradations: 1 µm)
	Illuminator	Built-in Koehler illumination for transmitted light, Light preset switch, Light intensity LED indicator, Built-in filters (LBD-IF, ND6, ND25, optional) 12 V 100 W halogen bulb (pre-centered)
Revolving nosepiece		Interchangeable reversed quintuple/coded quintuple/sextuple/septuple/coded septuple nosepiece
Observation tube	Widefield (F.N. 22)	• Widefield tilting trinocular • Widefield trinocular • Widefield tilting binocular • Widefield tilting,Telescopic,Lifting binocular • Widefield ergo binocular • Widefield binocular
	Super widefield (F.N. 26.5)	• Super widefield trinocular • Super widefield erect image trinocular
Stage		Ceramic-coated coaxial stage with left or right hand low drive control: with rotating mechanism and torque adjustment mechanism, optional rubber grips available (Non stick grooved coaxial, plain, rotatable stages are also available)
Condenser		• Abbe (N.A. 1.1), for 4x–100x • Swing out Achromatic (N.A. 0.9), for 1.25x–100x (swing-out: 1.25x–4x) • Achromatic Aplanatic (N.A. 1.4), for 10x–100x • Phase contrast, darkfield (N.A. 1.1), [phase contrast: for 10x–100x, darkfield: for 10x–100x (up to N.A. 0.80)] • Universal (N.A. 0.9), for 1.25x–100x [swing-out: 1.25x–4x, with oil top lens:(N.A. 1.4)] • Low (N.A. 0.75), for 2x–100x (Dry) • Ultra low (N.A. 0.16), for 1.25x–4x • Darkfield dry (N.A. 0.8–0.92), for 10x–100x • Darkfield oil (N.A. 1.20–1.40), for 10x–100x
Fluorescence illuminator		• Multi-purpose coded type (F.N. 22, 8-position mirror unit turret, 4-position ND slider) • Economical type (F.N. 26.5, 8-position mirror unit turret)
Fluorescence light source		100 W Hg apo lamp housing and transformer, 100 W Hg lamp housing and transformer or 75 W Xe lamp housing and transformer

The U-CBM is designed for the BX3 use in industrial environments for the EMC performance (IEC61326-1 Class A device). Using it in a residential environment may affect other equipment in the environment.

BX43/BX46/BX53 common specifications

Operating environment	• Indoor use • Ambient temperature : 5 ° to 40 °C (41 ° to 104 °F) • Maximum relative humidity : 80 % for temperatures up to 31° C (88 °F), decreasing linearly through 70 % at 34 °C (93 °F), 60 % at 37 °C (99 °F), to 50 % relative humidity at 40 °C (104 °F) • Supply voltage fluctuations : Not to exceed ±10 % of the normal voltage

3.3. Specification of Work pieces and Properties of Work Materials

3.3.1.Stainless Steel (AISI304)

Table 3.9:Dimensions of AISI304 Stainless Steel specimen

LENGTH	BREATH	THICKNESS
7.5 cm	8 cm	0.5 cm

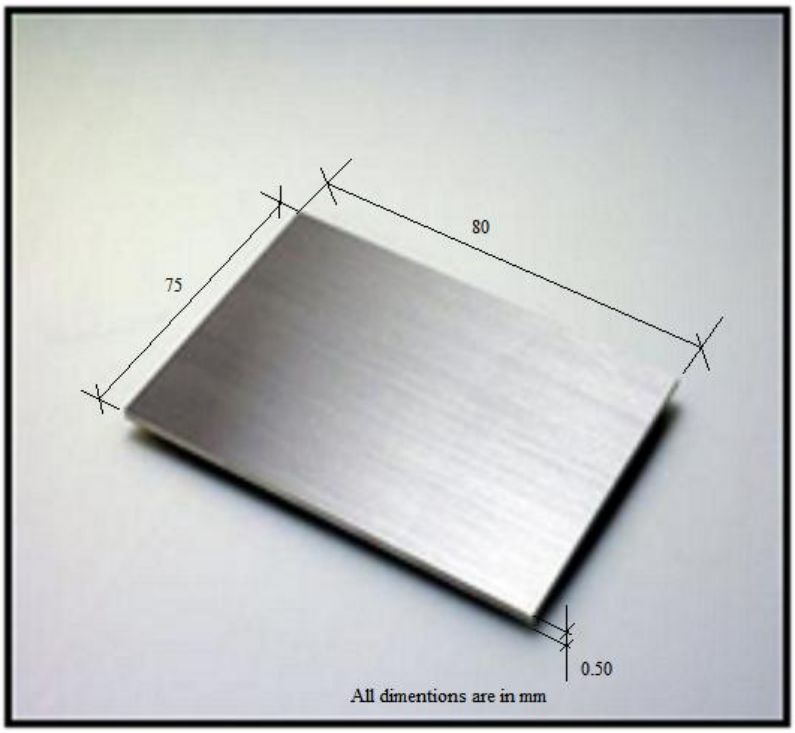

Fig 3.3: Stainless Steel (AISI304)

3.3.2. Functional Graded Material (FGM)

Table 3.10:Dimensions of Functionally Graded Material (FGM) Specimen

LENGTH	BREATH	THICKNESS
15 cm	25 cm	8 mm(1 mm each layer)

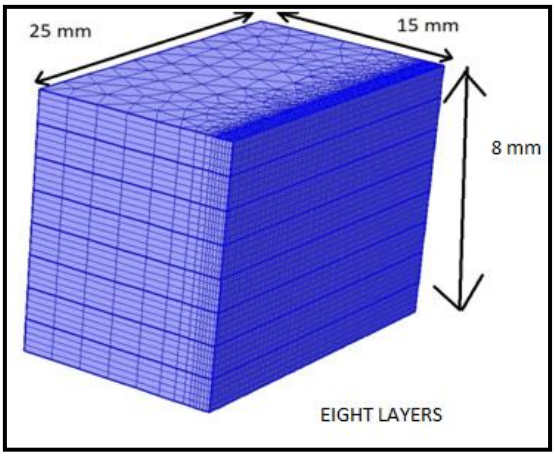

Fig 3.4: Functionally Graded Material (FGM)

3.4. Numerical and Experimental Plans

Firstly, in case of laser cutting (numerical simulation and experimental)of stainless specimens two parameters (laser power and scanning speed) have been considered. Details of the above parameters chosen are given in the following tables.

Table 3.11: Details of Input Parameters for Experimental and Numerical Simulation at Different Laser Scanning Speed.

Sl No	Laser Power (W)	Scanning Speed (mm/s)
1	90	1
2	90	2
3	90	3
4	90	4
5	90	5

Table 3.12: Details of Input Parameters for Experimental and Numerical Simulation at Different Laser Power

Sl No	Laser Power (W)	Scanning Speed (mm/s)
1	90	1
2	85	2
3	80	3
4	75	4
5	70	5

Secondly, in case of laser cutting (numerical simulation) of FGM material two input parameters have been considered. Those are Laser power and scanning speed. Details of the above parameters chosen are given in the following tables.

Table 3.13: Details of Input Parameters Numerical Simulation at Different Laser Power

Sl No.	Laser Power (W)	Scanning Speed (mm/s)
1	200	5
2	250	5
3	300	5
4	350	5
5	400	5
6	500	5
7	600	5
8	700	5
9	800	5
10	900	5
11	1000	5
12	1100	5
13	1200	5
14	1300	5
15	1400	5
16	1500	5
17	1600	5

Table 3.14: Details of Input Parameters Numerical Simulation at Different Laser Scanning Speed

SL No.	Laser Power (W)	Scanning Speed (mm/s)
1	400	2.5
2	400	5
3	400	7.5
4	400	10

3.5. Experimental and Numerical Simulation Procedure:

The present study is to investigate some aspects of through laser cutting of stainless steel, emphasis the effect of some important parameter on the quality of cut. The input parameters taken into consideration are laser power and scanning speed of the beam. In this work, the dimension of the specimen is 75 mm ×80 mm × 0.5 mm.

After cutting, the quality of cut has been analysed by measuring the width and depth of cut line under optical microscope The experimental results are verified using simulation results with the help of Comsol multiphysics 5.3a software and the deviation of the results are discussed and interpreted.

The effect of process parameters viz. laser power and scanning speed on kerf width, depth of cut , thermal stress field are analyzed through numerical simulation investigations. Power law is used to find the characteristics of different layers of Functionally Graded Material. The entire thermo-mechanical simulation is carried out in COMSOL MULTIPHYSICS 5.3a, finite element software. The depth, width are obtained from numerical simulation.

3.6 Comsol Multiphysics

COMSOL Multiphysics is a wide ranging simulation user-friendly software for a wide range of applications. It is based on finite element software which provides conventional physics user interface and couple system of PDE (Partial Differential Equation).COMSOL gives an IDE and united work flow for chemical, electrical and mechanical applications.

COMSOL Server is the engine and software for running mathematical simulation apps and the platform for controlling their distribution and deployment. User developed applications can be run in COMSOL Server through a Windows-installed client or web browsers.

COMSOL was created in July 1986 by Svante Littmarck and Farhad Saeidi at the Royal Institute of Technology (KTH) in Stockholm, Sweden.

In the present simulation Laser is considered as a heat source and due to thermal gradient induced stress is developed. To make more accurate results highly non linier solver is used and the model is designed by the below modules.

a) Structural Module

i. **Structural Mechanics Module**: It is dedicated to the analysis of mechanical structures that are subject to dynamic or static load. It can be used for a wide variety of analysis types, transient, including stationary, Eigen modal, quasi-static, parametric, buckling, frequency-response, and pre-stressed.

ii. **Nonlinear Structural Materials Module**: An add-on to the mechanical capabilities of the Structural Mechanics Module and the MEMS Module with nonlinear material models, including large strain plastic deformation capabilities.

b) Heat Transfer Module

It contains simulation tools to study the mechanisms of heat transfer model conduction, convection, and radiation – often in collaboration with other physics, such as structural mechanics, fluid dynamics, electromagnetic, and chemical reactions [48,49].

Chapter 4: Experimental and Numerical Simulation Investigation of Laser Cutting of Stainless Steel (AISI-304)

4.1. Introduction

Laser cutting is a thermo-mechanical process, considering laser beam as a heat source. Other than the conventional cutting, laser beam is much more accurate, quick productive and also precise [50].As there is no direct contact between equipment and work piece; so no chance material consumption and very easy to automate. Intense laser beam is equivalent to a concentrated heat source which produces fine narrow cut and less HAZ (Heat Affected Zone). The aforesaid process is highly suitable for stainless steel (AISI-304) having melting point around 1400°C.

On the other hand, Stainless steel-304 is austenitic alloy consists of carbon(0.055%), phosphorus(0.029%), manganese (1%), silicon(0.6%), sulphur (0.005%), chromium(18.28%) and nickel (8.48%)[4].Hence, heating and rapid cooling associated with laser cutting of stainless steel AISI-304 initiates grain refinement, phosphate, carbide, sulphide formation, known as HAZ[5-7]. It is an undesirable phenomenon which has some backlogs. Also, during laser cutting considering the temperature gradient, large thermal stress is develop which may exceed the yield point of the material and produce crack or fracture.

There are many effective parameters like laser power, scanning speed, focal position; assist gas cooling and pressure etc make great impact on the laser cutting process [51, 31]. Laser power and scanning speed are the most important parameters for laser cutting of stainless steel. In order to minimize the HAZ and thermal stress the aforesaid process parameters play a crucial role in cut quality.

4.2. Theoretical Equations for Stainless Steel (AISI-304) Model

The temperature dependent material properties are given by Eq. (4.1) [52].

$$P = P_0(P_{-1}T^{-1} + 1 + P_1T + P_2T^2 + P_3T^3) \quad (4.1)$$

Where P_0, P_{-1}, P_1, P_2 and P_3 are the temperatures co-efficients. Both the mechanical and thermal problems are solved in our model. Coordinates and temperature affects on the mechanical properties.

Using the above Eq.(4.1), material properties of Stainless Steel (AISI-304)is shown in Table 4.1.

Table 4.1: Thermo-Mechanical Properties of Stainless Steel (AISI-304)

Temperature (K)	Thermal conductivity (W/(m·K))	Poisson's ratio	Specific heat (J/(kg.K))	Modulus of elasticity (Pa)	Coefficient of thermal expansion (1/°C)
300	12.14291852	0.317756	390.3507	2.07788E+11	1.5321E-05
500	12.31415754	0.324512	377.4911	1.9915E+11	1.7315E-05
636	13.17185401	0.334766	386.7647	1.87274E+11	1.86709E-05
700	12.14291852	0.317756	394.6853	1.80004E+11	1.5321E-05
750	13.72623579	0.341177	402.0421	1.73575E+11	1.9309E-05
800	14.21065256	0.346891	410.1856	1.6649E+11	1.98075E-05
850	14.73096585	0.353225	418.8973	1.58748E+11	2.0306E-05
900	15.84595719	0.36775	427.9589	1.50349E+11	2.1303E-05
950	16.42397287	0.375942	437.1521	1.41293E+11	2.18015E-05
1000	17.0045603	0.384753	446.2585	1.31581E+11	2.23E-05
1050	17.5793883	0.394183	455.0597	1.21211E+11	2.27985E-05
1100	18.14012567	0.404233	463.3375	1.10185E+11	2.3297E-05
1150	18.67844123	0.414901	470.8734	98502262040	2.37955E-05
1200	19.18600378	0.426189	477.4492	86162527360	2.4294E-05
1250	19.65448215	0.438097	482.8464	73165995000	2.47925E-05
1300	20.07554514	0.450623	486.8467	59512664960	2.5291E-05
1350	20.44086155	0.463769	489.2318	45202537240	2.57896E-05
1400	12.14291852	0.317756	489.7833	30235611840	1.5321E-05
1450	12.04024044	0.318516	488.2829	14611888760	1.58195E-05

4.3. Stainless Steel (AISI-304) Model Assumptions

In the present finite element model some assumptions are made as follows:

Laser hits the top surface of the specimen perpendicularly and the nature of the beam is lower order Gaussian mode(TEM_{00}). The Gaussian distribution of laser beam on the specimen is expressed by Eq. (4.2) [30],

$$q(x,y) = I_0 A \exp\left(-\frac{x^2 + y^2}{r^2}\right) \tag{4.2}$$

Where, I_0: beam intensity in watt/m^3, P: laser power in watt, A: co-efficient of absorption, r: radius of the beam in meter.

In the numerical study some other assumptions are given below.

a) Diameter of the laser beam is equal throughout the thickness of the specimen.
b) There is no effect of the assist gas such as gas pressure, cooling effect etc. and also the effect of molten layer is negligible.
c) The temperature of atmosphere is 300 K .
d) The natural convection takes place due to the surrounding atmosphere and the convective heat transfer coefficient is 10 W/m^2K.
e) The absorptivity of stainless steel (AISI304) varies from 0.20 to 0.645 [53-56]. In the present study absorptivity of stainless steel (AISI304) is considered as 0.645.
f) The top and the bottom surfaces are considered as a diffuse surface. Hence, the radiation heat transfer occurs and the emissivity is considered as0.355.
g) The melting point of stainless steel is considered as 1800K and 1100 K is considered as a Heat affected zone (HAZ).

4.4. Heat Transfer Analysis Model

In the Fourier's law, the 3D transient heat conduction model is represented by Eq. (4.3) [57].

$$\rho c\left(\frac{\partial T}{\partial t} + V\frac{\partial T}{\partial t}\right) = \frac{\partial}{\partial x}\left(K\frac{\partial T}{\partial x}\right) + \frac{\partial}{\partial y}\left(K\frac{\partial T}{\partial y}\right) + \frac{\partial}{\partial z}\left(K\frac{\partial T}{\partial z}\right) + Q_G \tag{4.3}$$

Where, K: Thermal conductivity (W/m.K), c:Specific heat (J/kg.K),ρ:Density (kg/m^3), V : Velocity (m/s),Q_G: Rate of heat generation (W/m^3).Initial boundary condition of the specimen is shown by Eq. (4.3).

$$T(x,y,z,0) = T_0 \tag{4.4}$$

Where T_0: Ambient temperature (300 K). The free convection to atmosphere is considered as per Eq. (4.5) at bottom, top and lateral surfaces and the general boundary condition.

$$Q_{convec} = h(T_s - T_0) \tag{4.5}$$

Where h: Convective heat transfer coefficient (W/m^2K),T_s : Surface temperature(^0C). The radiation heat loss is considered on the top and the bottom surface and the general boundary condition.

$$Q_{rad} = \in \sigma A(T^4 - T_0^4) \tag{4.6}$$

Where $\in$: emissivity of the material,σ: Stefan–Boltzmann constant,A:Surface area.

The energy required for melting can be expressed by the Eq. (4.7).

$$E = \frac{\pi D^2}{4}\rho vt[C(T_M - T_0) + L] \tag{4.7}$$

Where, E: Energy required to melt (J), D: Diameter of laser beam (m), ρ: Density of the specimen (kg/m^3),v: Penetration speed (m/s), t:Time(s), C: Specific heat(J/kg.K),T_M: Melting temperature (K), T_0: Ambient temperature (300 K), L: Latent heat of fusion (J/kg).

4.5. Thermal Stress

In the fusion cutting heat associated is concentrated in a very small region. When the laser beam is focused on the top surface, the temperature of that region is heated up. As a result, the surrounding surface gives compressive force on that region (due to low temperature of the surrounding).Due to the temperature variation thermal stress is developed [58].

$$\sigma_{TH} = \frac{E\alpha\Delta T}{1 - v} \tag{4.8}$$

Where, E: Young's modulus,α: coefficient of thermal expansion,v: Poisson's ratio. The Von mises stress is given by the following expression.

$$\sigma = \sqrt{\frac{(\sigma_1 - \sigma_2)^2 + (\sigma_2 - \sigma_3)^2(\sigma_1 - \sigma_3)^2}{2}} \tag{4.9}$$

Where $\sigma_1, \sigma_2, \sigma_3$ are the three principal stress of principal axis(X, Y, Z axis).

4.6. Meshing & Solutions

The beam hits on the X-Z plane and travels along the X direction while the kerf is generated in the Z direction. The simulation is done on the half of the specimen and uses symmetry property about Y axis to minimize computational time. Dimension of the work piece is modelled as 75mm × 80mm × 0.5 mm (X × Y × Z). Taking into consideration of the same mesh; two different types of elements are considered in this present simulation study. In case of mesh analysis, triangle type element is used on the top plane and 'Swift' option is used to copy the mesh in the whole specimen.

The density of the mesh has a large impact on the simulation results. High coarseness of mesh size leads to more erroneous results but needs less computational time. Whereas the high fineness of mesh size provides more accurate results but needs more computational time. When the path is fine mesh, in that portion more accurate results are found even though computational time is more whereas the other part of specimen (ineffective part) which is coarse mesh decreases the computational time but can lead to less accurate results. In this nonlinear mesh model, total numbers of 33885elements are considered. The travelling beam (heat flux) is simulated by varying the time steps. In the COMSOL there is no element death methodology is considered. Hence, by putting the value of young's modulus as close to 0 and the Poisson ratio as close to 0.5, the elements reach above the melting point are no longer taking part in any kind of interaction.

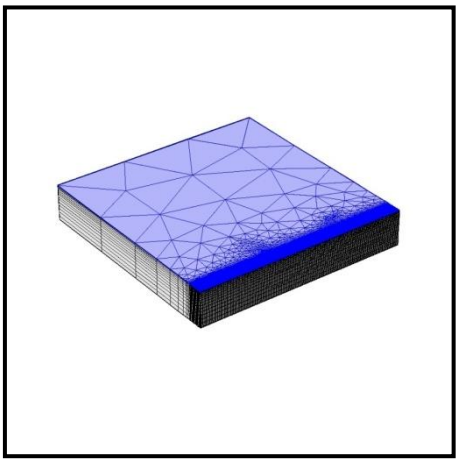

Fig. 4.1: Mesh Structure (combination of fine and coarse mesh) of stainless steel(AISI-304).

4.7. Results and Discussion

4.7.1. Experimental Observations

Experimental set up, plan and procedure have been discussed in the previous chapter. In this chapter results are given and discussed. Different experimental data analysis has been reported. Width of cut and depth of cut are considered in the analysis. Pictorial view of typical laser cutting sample on stainless steel (AISI-304) sample is shown in Fig.4.2 .For observing depth of cut and width of cut stainless steel (AISI-304) sample are cold mounted using an araldite solution. Pictorial views of polished laser cutting specimens and mounted samples containing two laser cutting specimens are shown in Fig 4.3 (a) and (b).

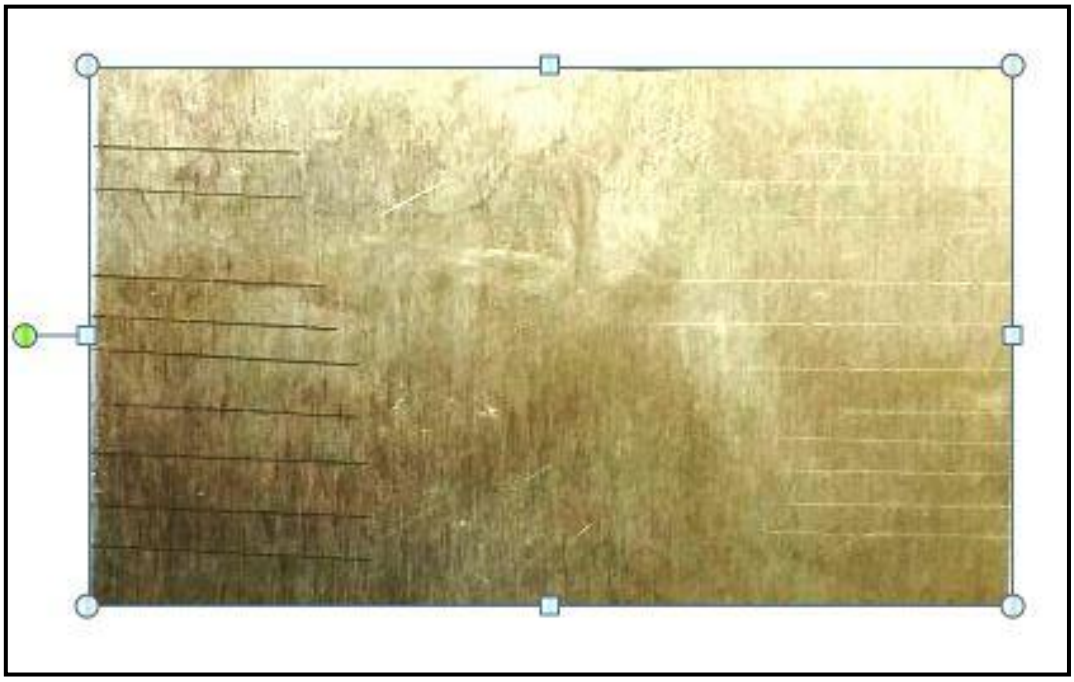

Fig. 4.2: Photographic views of typical laser cutting sample of Stainless steel (AISI-304).

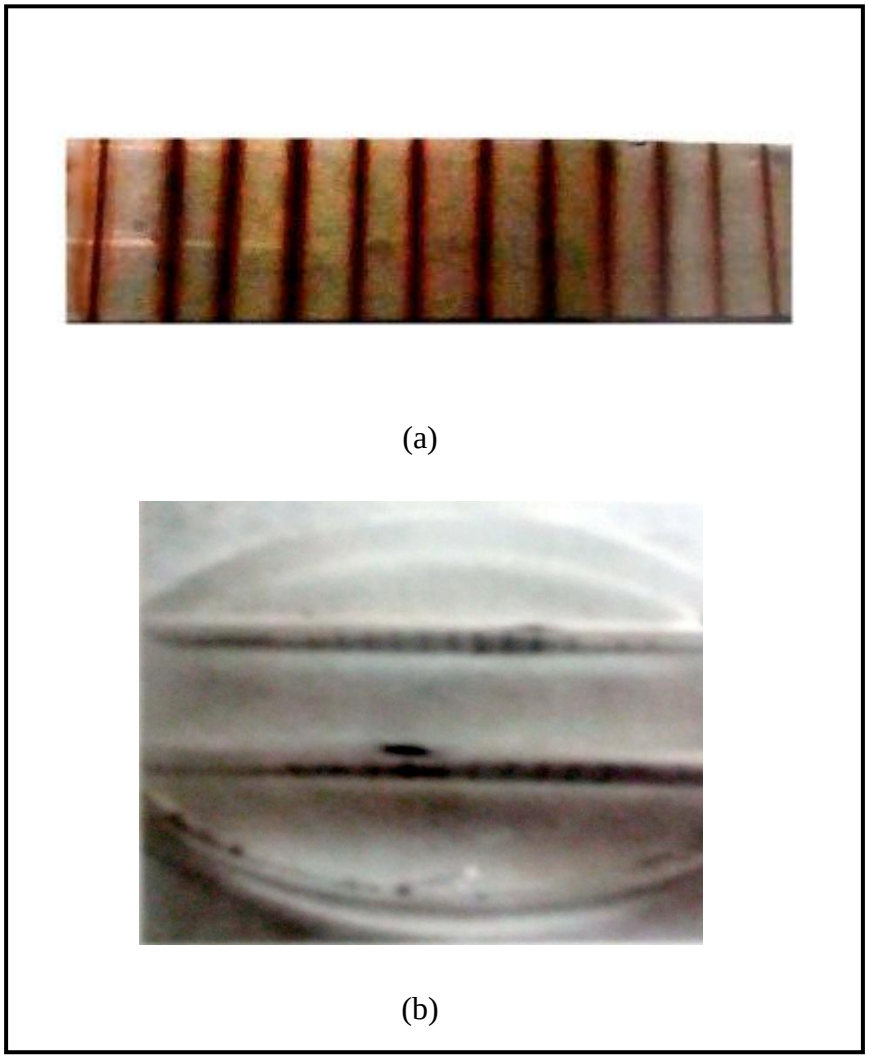

(a)

(b)

Fig. 4.3:(a) Photographic view of polished laser cutting of stainless steel (AISI-304)specimen and (b) mounted samples containing two laser cutting specimens. .

Measurements of kerf width and depth of cut for different laser powers and scanning speeds under optical microscope are shown in Figs 4.4. (a),(b),(c) and (d).

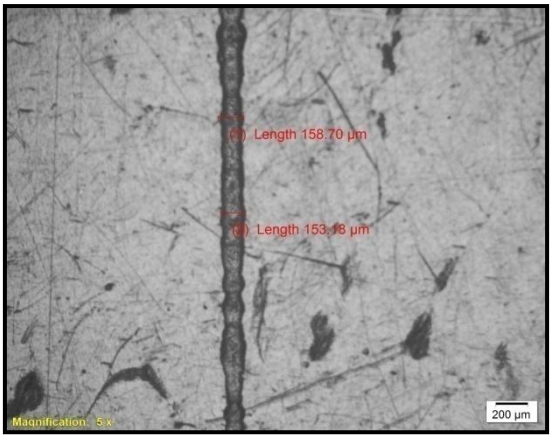

(a) Power: 80% of 9.28W, Scanning Speed:1 mm/s

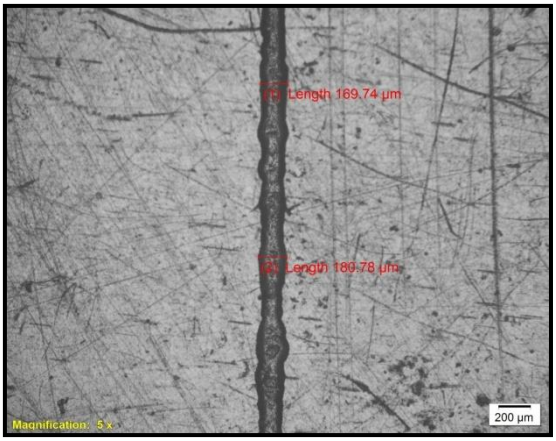

(b) Power: 85% of 9.28W,Scanning Speed:1 mm/s

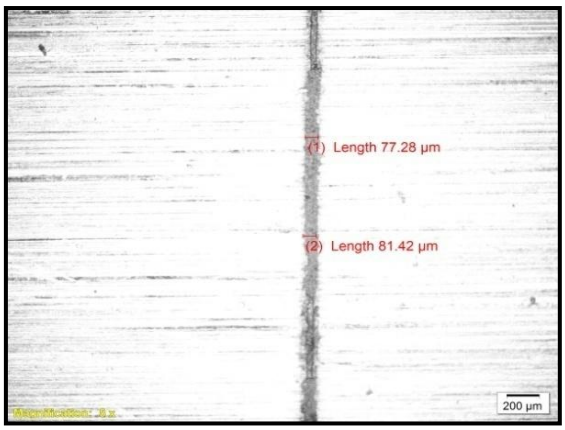

(c) Power:75% of 9.28W,Scanning Speed:1mm/s

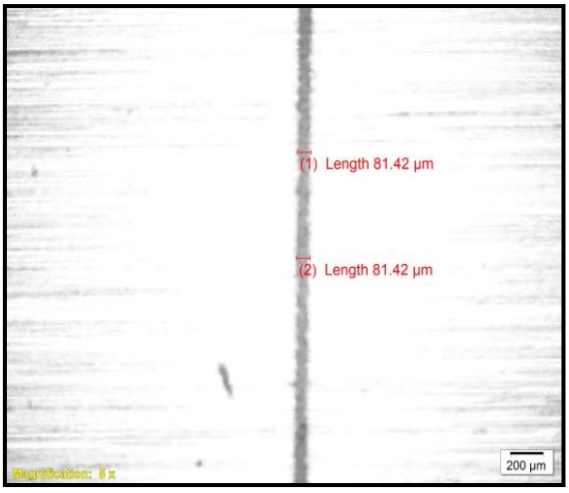

(d) Power: 90% of 9.28 W, Scanning Speed:5mm/s

Fig. 4.4: Measurement of width and depth of cut as done under optical microscope for (a)Power: 80% of 9.28 W, Scanning Speed:1 mm/s, (b) Power: 85% of 9.28W,Scanning Speed:1 mm/s,(c) Power:75% of 9.28W,Scanning Speed:1mm/s and(d) Power: 90% of 9.28W,Scanning Speed:5mm/s.

4.7.2. Temperature Profile Analysis

In this present study a finite element simulation model is established to describe the sublimation laser cutting on stainless steel (AISI-304).The simulated model is verified by the experimental results and the effects of laser power and scanning speed on the thermal stress, kerf width and depth of cut are analysed.

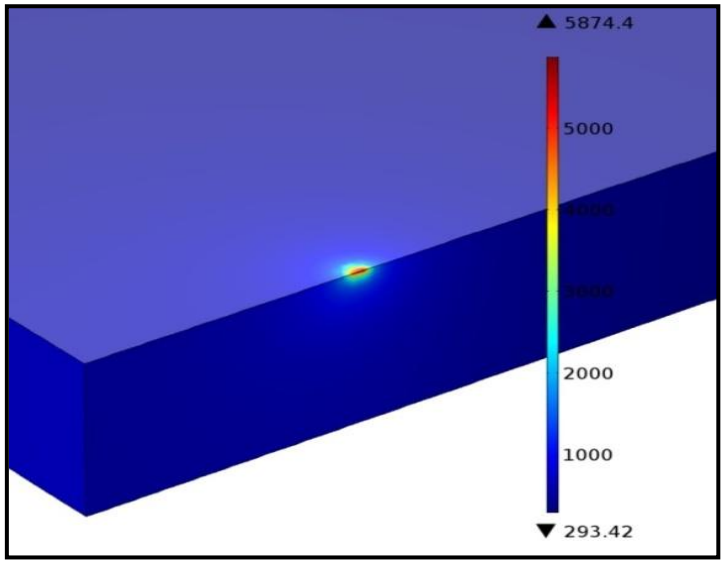

Fig. 4.5: Temperature distribution profile

The three dimensional view of temperature profile of sublimation cutting is shown in Fig 4.5. It is observed that along the Y axis temperature decreases gradually with the increase of distance from the top surface of the specimen as shown in Fig 4.6.

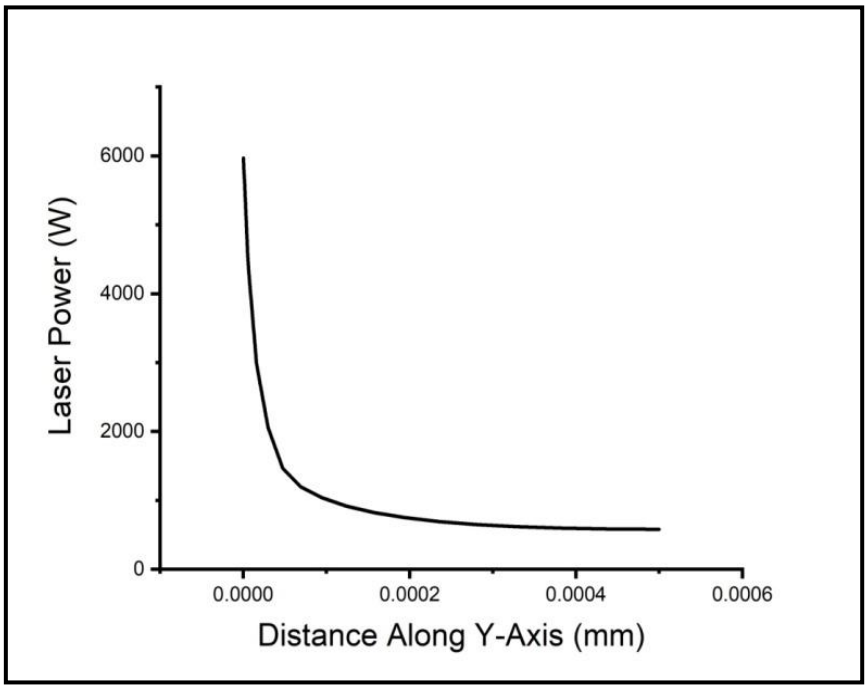

Fig. 4.6: Temperature vs. Distance plot for laser machining of Stainless Steel(AISI-304) at cutting speed : 3mm/sec and laser power : 90% of 9.28Watt.

The temperature of a point along the cutting line varies at different time is shown in Fig. 4.7.

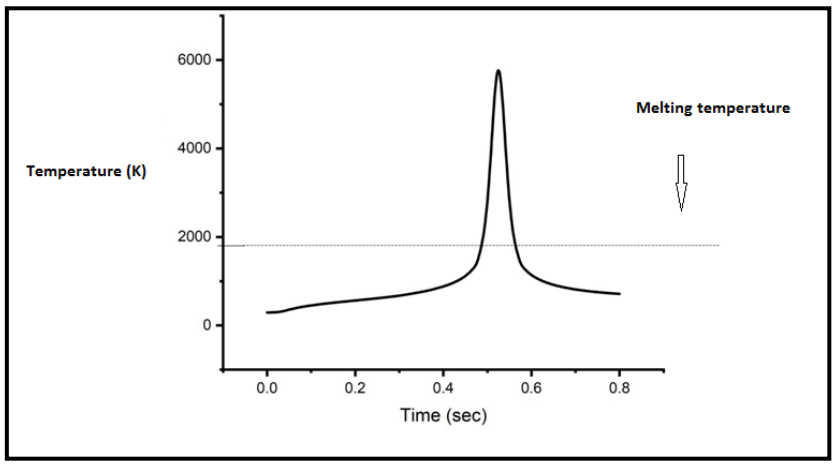

Fig. 4.7: Temperature vs time along the cutting line

4.7.3. Comparative study of width of cut, depth of cut and HAZ obtain from Experimental and Numerical results

Table 4.2 and 4.3 shows the Comparative study between Width of cut, depth of cut and HAZ of Stainless Steel (AISI-304) obtain from Experimental and Numerical results at different Laser power and Scanning speed.

Table 4.2: Comparative study of Width of cut, depth of cut and HAZ of Stainless Steel (AISI-304) obtain from Experimental and Numerical results at different Laser Scanning speed.

Sl. No	Laser Power (W) (%)	Scanning Speed (mm/s)	Experimental Width (mm)	Experimental Depth (mm)	Experimental HAZ (mm)	Simulation Width (mm)	Simulation Depth (mm)	Simulation HAZ (mm)
1	90	1	0.1067	0.04089	0.19016	0.098	0.042	0.194
2	90	2	0.08604	0.03928	0.17971	0.09	0.04	0.18
3	90	3	0.08564	0.03862	0.16746	0.084	0.037	0.164
4	90	4	0.08188	0.03210	0.15790	0.082	0.034	0.16
5	90	5	0.08142	0.02986	0.15698	0.08	0.03	0.156

Table 4.3: Comparative study of Width of cut and Depth of cut of Stainless Steel (AISI-304) from Experimental and Numerical results at different Laser Power

Sl. No	Laser Power % (W)	Scanning Speed (mm/s)	Experimental Width	Experimental Depth	Experimental HAZ	Simulation Width	Simulation Depth	Simulation HAZ
1	90	1	0.09764	0.04628	0.19832	0.098	0.042	0.194
2	85	1	0.08451	0.03522	0.17526	0.086	0.036	0.178
3	80	1	0.08425	0.03492	0.15593	0.08	0.034	0.154
4	75	1	0.07935	0.03146	0.15377	0.078	0.033	0.152
5	70	1	0.07189	0.03022	0.14468	0.072	0.032	0.142

The contribution of the laser power and scanning speed on the kerf width and depth of cut are identified with the help of parametric study as shown in Fig. 4.8 and 4.9.Keeping other parameters unchanged laser cutting is performed by several different laser powers and scanning speeds. The simulation results show good argument with the experimental results.

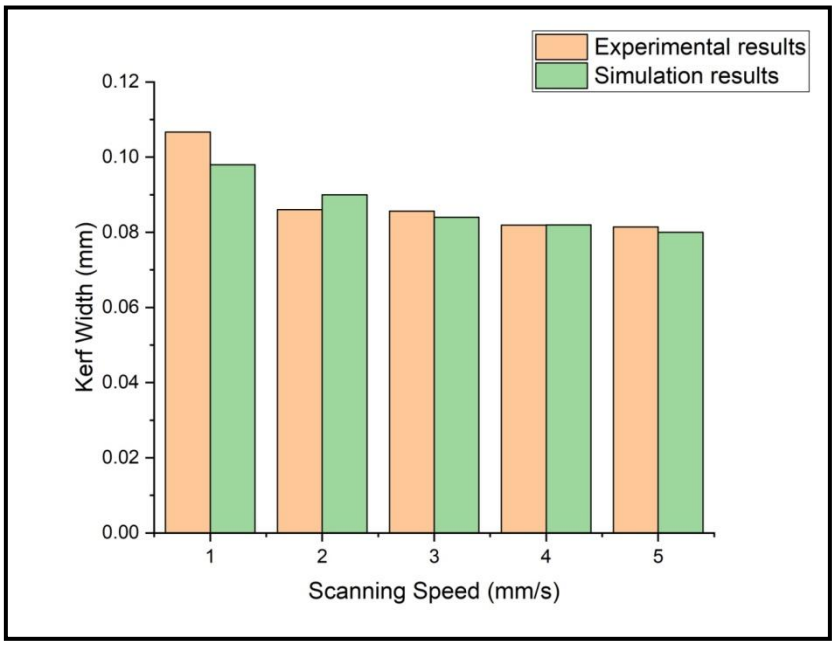

(a) Scanning Speed (mm/s) vs Kerf Width(mm)

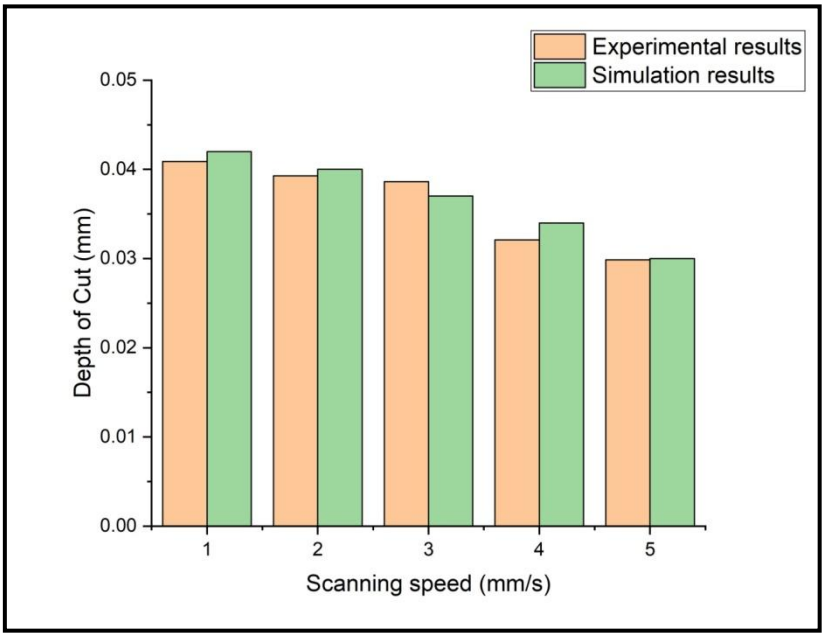

(b) Scanning Speed (mm/s) vs Depth of Cut (mm)

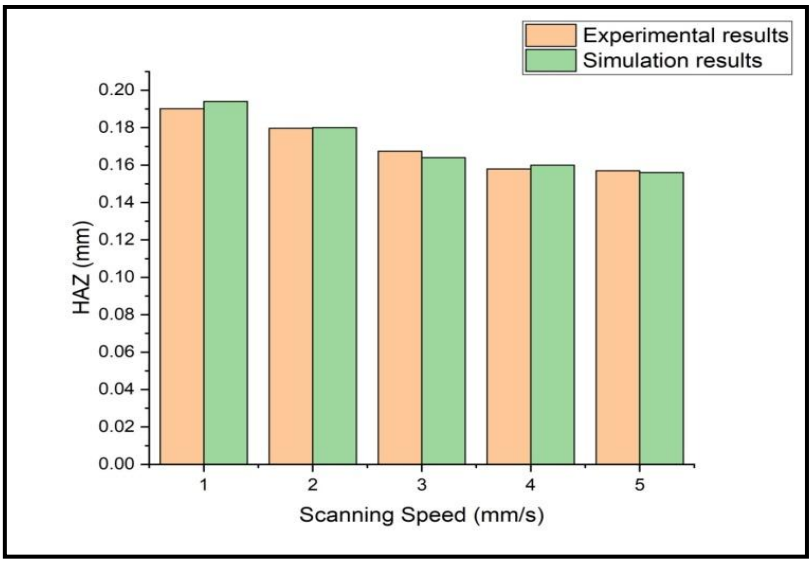

(c)Scanning Speed (mm/s) vs HAZ (mm)

Fig. 4.7: Comparative study between Width of cut, depth of cut and HAZ of Stainless Steel (AISI-304) obtain from Experimental and Numerical results at different Laser Scanning speed.

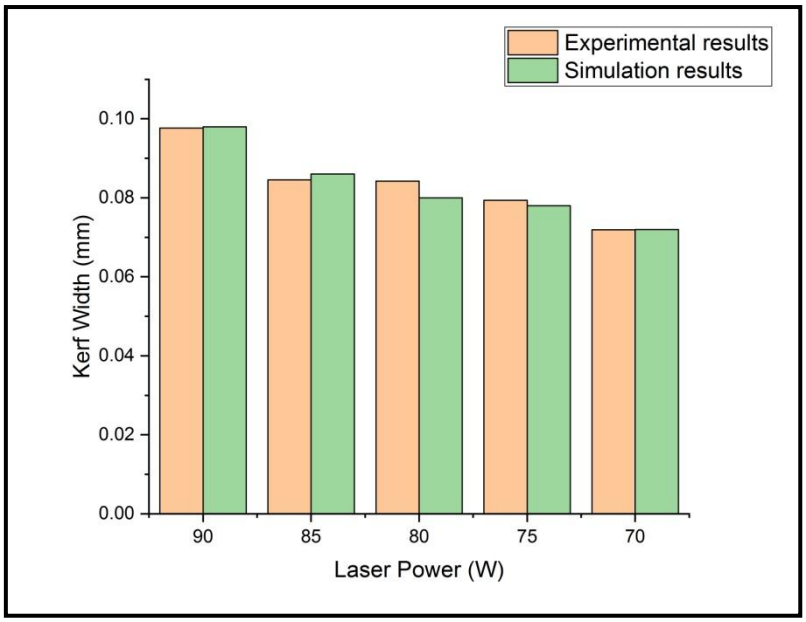

(a) Laser Power(%) vs Kerf Width(mm)

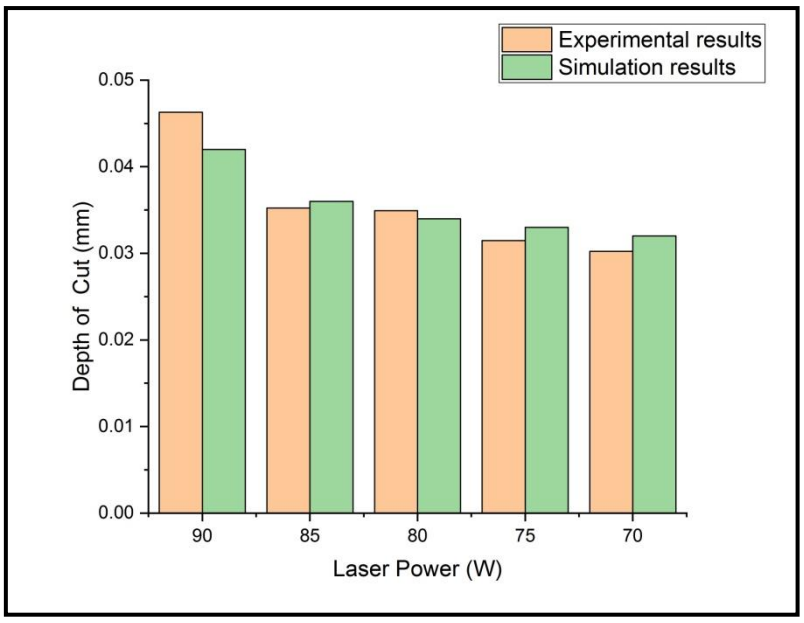

(b) Laser Power(%) vs Depth of Cut (mm)

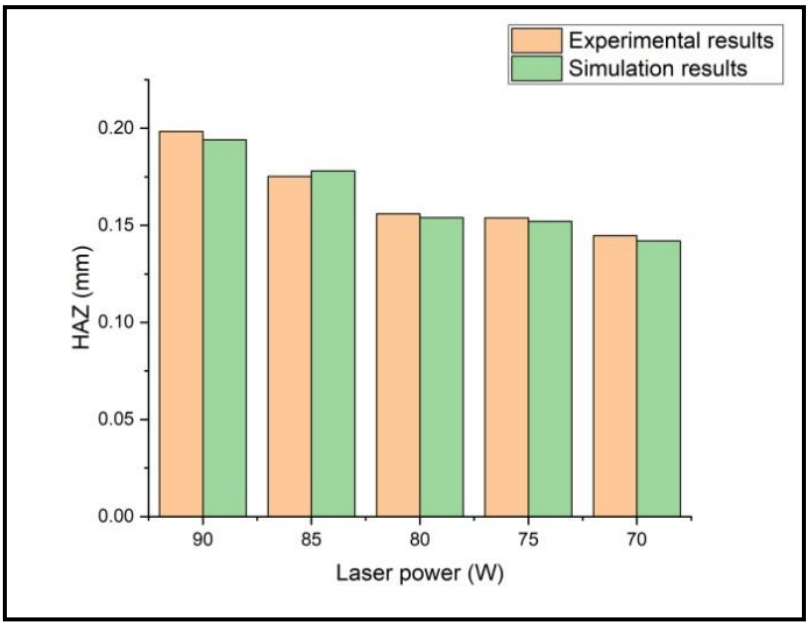

(c)Laser Power(%) vs HAZ (mm)

Fig. 4.8: Comparative study of Width of cut and Depth of cut of Stainless Steel (AISI-304) from Experimental and Numerical results at different Laser Power

4.8. Conclusions

Laser cutting of 0.5 mm thick stainless steel-304 sheet was performed by using finite element numerical analysis to predict kerf width and depth of cut. The results of numerical mathematical model were validated by experiment results. Comsol multiphysics 5.3a was used to simulate the lower order Gaussian heat source and putting Young's modulus tends to zero and Poisson ratio 0.5 element death methodology was employed for material removal. The proposed thermo-mechanical simulation was a combination of heat transfer and solid mechanics (mechanical) analysis. The simulation results of heat transfer analyse show that the kerf width increases with an increase in laser power and decreases with an increase in scanning speed. Moreover the temperature rises sharply near the focused laser beam. However, temperature gradient decreases gradually and sharply with the increase of distance from the cutting edge. From the solid mechanics analysis the results of thermal stress was identified. It was found that maximum stress concentrations were observed at the cutting edge especially at the middle of the specimen which was supported by the analysis of optical microscope.

Chapter 5: Numerical simulation investigation of Laser Cutting on Functionally Graded Material (Ni-SS)

5.1. Introduction

The functional graded material (FGM) is a special type of composite material which is widely used in engineering applications as it is free from de-bonding and de-lamination effects unlike composite materials [2]. Due to wide use of such material, different machining techniques of such material is a promising area of research. Among the entire machining techniques laser cutting finds prime significance in FGMs for better accuracy and in the applications where objects require very high precision [3]. Laser cutting process is a novel method for machining FGM material which is extensively used in aerospace, automobile, biomedical, defense, electrical or electronic, energy, marine opto-electronics, and thermo-electronics etc. In 1967, this laser cutting method was first practically implemented for conventional materials. But the first time this method was used in aerospace engineering in the year 1970. Recently, laser cutting is used mainly for its fine narrow cutting and moreover ease of controlling the entire process. Generally, fusion and sublimation cutting are mainly used in industrial practices over long period of time. In case of fusion cutting, the molecules of the material are directly converted to the vapor state from the solid state. Some assist gases like nitrogen and oxygen are used to remove the vapor molecules during the process [33, 30]. The nitrogen gas is mainly used as an inert gas which is used to protect the oxidization by creating a shield which prevents contact with atmospheric oxygen [29, 20]. The oxygen gas is used as an external heat source which helps to cut the material. In the sublimation cutting technique the molecules of the material is firstly converted to molten state from solid state and then the molten material is converted to vapor [30, 59]. On the other hand, for fusion laser cutting the laser beam hits on the top surface of the specimen and some portion of beam is absorbed by the specimen. Some part of the absorbing heat is transferred from the point of incident laser beam and the other part of the heat increases the temperature of that part. When the temperature reaches the melting point of the material, the specimen gets melted. The molten layer is removed from the specimen and makes cut kerf. For the present analysis

rectangular plate of FGM material made of nickel (Ni)-stainless steel (AISI 304) is considered. For the simplification absorptivity and the reflectivity of FGM material are taken as 0.465 and 0.535 respectively.

5.2. Theoretical Equations for FGM Model

The FGM rectangular block is established in the model section and the properties of the material is assumed to The Power Law is shown in Eq. (5.1) and Eq. (5.2) [60].

$$p(z) = (p_{ni} - p_{ss})V_{ni} + p_{ss} \tag{5.1}$$

$$V_{ni} = \left(\frac{1}{2} + \frac{z}{h}\right)^{n} [n \geq 0] \tag{5.2}$$

where P is the effective material properties such as density(ρ), coefficient of thermal expansion(α), poisson's ratio (μ), thermal conductivity (k), Young's modulus (E); the "ni" and "ss" represent as Nickel and stainless steel respectively ; V is the volume fraction of the nickel and "n" is the volume fraction exponent considered as one in present numerical investigation. The temperature dependent material properties are given by Eq. (4.3) [61].

$$P = P_0(P_{-1}T^{-1} + 1 + P_1T + P_2T^2 + P_3T^3) \tag{5.3}$$

Where P_{-1} ,P_0, P_1, P_2 and P_3 are the temperature co-efficients .Both the mechanical and thermal problems are solved in the present model. Coordinates and temperature affects on the mechanical properties.

Using the above Eq. 5.1, 5.2 and 5.3 the material properties of Functionally graded material which contains eight layers are shown in following tables [60,61].

Table 5.1: Thermo-mechanical properties of top layer of FGM

Temperature (K)	Thermal conductivity (W/(m.K))	Poisson's ratio	Specific heat (J/(kg.K))	Modulus of elasticity (Pa)	Coefficient of thermal expansion (1/°C)
300	83.729951	0.31	431	2.052E+11	1.25117E-05
500	59.830699	0.31	505	1.928E+11	1.4239E-05
636	55.062357	0.31	524	1.845E+11	1.54135E-05
700	55.910958	0.31	531	1.805E+11	1.59662E-05
750	56.690908	0.31	523.494136	1.775E+11	1.6398E-05
800	57.566135	0.31	526.431008	1.744E+11	1.68298E-05
850	58.529927	0.31	530.266331	1.714E+11	1.72616E-05
900	59.575574	0.31	534.926391	1.683E+11	1.76934E-05
950	60.696365	0.31	540.337476	1.653E+11	1.81252E-05
1000	61.885588	0.31	546.425874	1.622E+11	1.8557E-05
1050	63.136532	0.31	553.11787	1.592E+11	1.89889E-05
1100	64.442485	0.31	560.339751	1.562E+11	1.94207E-05
1150	65.796738	0.31	568.017806	1.531E+11	1.98525E-05
1200	67.192578	0.31	576.078321	1.501E+11	2.02843E-05
1250	68.623294	0.31	584.447582	1.471E+11	2.07161E-05
1300	70.082176	0.31	593.051878	1.441E+11	2.11479E-05
1350	71.562512	0.31	601.817494	1.411E+11	2.15797E-05
1400	73.057590	0.31	610.670718	1.381E+11	2.20115E-05
1450	74.560700	0.31	619.537837	1.351E+11	2.24433E-05
1500	76.065131	0.31	628.345138	1.321E+11	2.28751E-05
1550	77.564171	0.31	637.018908	1.291E+11	2.33069E-05
1600	79.051109	0.31	645.485434	1.261E+11	2.37387E-05
1650	80.519234	0.31	653.671002	1.231E+11	2.41705E-05
1700	81.961835	0.31	661.501901	1.201E+11	2.46023E-05
1750	83.372201	0.31	668.904416	1.171E+11	2.50342E-05
1800	84.743620	0.31	675.804835	1.142E+11	2.5466E-05

Table 5.2: Thermo-mechanical properties of second layer from the top of FGM

Temperature (K)	Thermal conductivity (W/(m.K))	Poisson's ratio	Specific heat (J/(kg .K))	Modulus of elasticity (Pa)	Coefficient of thermal expansion (1/°C)
300	70.30738	0.31145	423.3783	2.06E+11	1.3E-05
500	50.92135	0.31272	481.0921	1.94E+11	1.48E-05
636	47.20789	0.31464	498.2684	1.85E+11	1.6E-05
700	47.70445	0.31145	505.441	1.8E+11	1.58E-05
750	48.63503	0.31584	500.7219	1.77E+11	1.69E-05
800	49.43698	0.31691	504.635	1.73E+11	1.74E-05
850	50.31762	0.31810	509.3846	1.69E+11	1.78E-05
900	51.37627	0.32082	514.87	1.65E+11	1.84E-05
950	52.39529	0.32236	520.9902	1.61E+11	1.88E-05
1000	53.4704	0.32401	527.6445	1.57E+11	1.93E-05
1050	54.59457	0.32578	534.732	1.52E+11	1.97E-05
1100	55.76079	0.32766	542.1518	1.48E+11	2.01E-05
1150	56.96206	0.32966	549.8032	1.43E+11	2.06E-05
1200	58.19135	0.33178	557.5854	1.38E+11	2.1E-05
1250	59.44164	0.33401	565.3974	1.33E+11	2.15E-05
1300	60.70593	0.33636	573.1384	1.28E+11	2.19E-05
1350	61.9772	0.33883	580.7077	1.23E+11	2.24E-05
1400	61.63609	0.31145	588.0043	1.18E+11	2.08E-05
1450	62.83811	0.31159	594.9275	1.13E+11	2.12E-05
1500	64.06044	0.31185	601.3765	1.07E+11	2.16E-05
1550	65.29605	0.31223	607.2503	1.01E+11	2.21E-05
1600	66.53793	0.31272	612.4481	9.57E+10	2.25E-05
1650	67.77907	0.31332	616.8692	8.98E+10	2.3E-05
1700	69.01244	0.31405	620.4127	8.39E+10	2.34E-05
1750	70.20664	0.31460	622.9777	7.78E+10	2.38E-05
1800	71.32391	0.31464	624.4635	7.16E+10	2.42E-05

Table 5.3: Thermo-mechanical properties of third layer from the top of FGM

Temperature (K)	Thermal conductivity (W/(m.K))	Poisson's ratio	Specific heat (J/(kg.K))	Modulus of elasticity (Pa)	Coefficient of thermal expansion (1/°C)
300	61.359	0.31242	418.2971	2.06E+11	1.34E-05
500	44.98178	0.31453	465.1535	1.95E+11	1.52E-05
636	41.97158	0.31773	481.114	1.85E+11	1.64E-05
700	42.23345	0.31242	488.4017	1.8E+11	1.58E-05
750	43.26445	0.31974	485.5404	1.76E+11	1.73E-05
800	44.01755	0.32152	490.1043	1.72E+11	1.78E-05
850	44.84275	0.32350	495.4635	1.67E+11	1.82E-05
900	45.91007	0.32804	501.499	1.63E+11	1.88E-05
950	46.86124	0.33060	508.092	1.58E+11	1.93E-05
1000	47.86027	0.33336	515.1236	1.53E+11	1.97E-05
1050	48.89992	0.33630	522.4747	1.47E+11	2.02E-05
1100	49.973	0.33944	530.0265	1.42E+11	2.06E-05
1150	51.07227	0.34278	537.6602	1.36E+11	2.11E-05
1200	52.19052	0.34630	545.2567	1.3E+11	2.15E-05
1250	53.32054	0.35003	552.6972	1.24E+11	2.2E-05
1300	54.4551	0.35394	559.8628	1.18E+11	2.24E-05
1350	55.587	0.35805	566.6345	1.11E+11	2.29E-05
1400	54.02176	0.31242	572.8934	1.04E+11	1.99E-05
1450	55.02306	0.31266	578.5207	9.74E+10	2.04E-05
1500	56.05731	0.31309	583.3973	9.03E+10	2.08E-05
1550	57.1173	0.31371	587.4045	8.3E+10	2.13E-05
1600	58.19581	0.31453	590.4233	7.54E+10	2.17E-05
1650	59.28562	0.31554	592.3347	6.76E+10	2.22E-05
1700	60.37952	0.31675	593.0199	5.97E+10	2.26E-05
1750	61.4296	0.31768	592.36	5.15E+10	2.3E-05
1800	62.37744	0.31773	590.2359	4.32E+10	2.33E-05

Table 5.4: Thermo-mechanical properties of fourth layer from the top of FGM

Temperature (K)	Thermal conductivity (W/(m.K))	Poisson's ratio	Specific heat (J/(kg.K))	Modulus of elasticity (Pa)	Coefficient of thermal expansion (1/°C)
300	52.41062	0.31339	413.2159	2.06E+11	1.37E-05
500	39.04221	0.31634	449.2149	1.96E+11	1.56E-05
636	36.73526	0.32083	463.9596	1.86E+11	1.68E-05
700	36.76244	0.31339	471.3623	1.8E+11	1.57E-05
750	37.89386	0.32364	470.3589	1.76E+11	1.77E-05
800	38.59811	0.32614	475.5736	1.71E+11	1.81E-05
850	39.36788	0.32891	481.5424	1.66E+11	1.86E-05
900	40.44387	0.33526	488.1281	1.6E+11	1.93E-05
950	41.32719	0.33885	495.1939	1.55E+11	1.97E-05
1000	42.25014	0.34270	502.6026	1.49E+11	2.02E-05
1050	43.20528	0.34683	510.2174	1.43E+11	2.07E-05
1100	44.1852	0.35122	517.9013	1.36E+11	2.11E-05
1150	45.18248	0.35589	525.5171	1.29E+11	2.16E-05
1200	46.1897	0.36083	532.9281	1.22E+11	2.2E-05
1250	47.19944	0.36604	539.9971	1.15E+11	2.25E-05
1300	48.20428	0.37152	546.5871	1.07E+11	2.3E-05
1350	49.19679	0.37727	552.5613	9.92E+10	2.34E-05
1400	46.40742	0.31339	557.7825	9.09E+10	1.91E-05
1450	47.208	0.31372	562.1138	8.24E+10	1.95E-05
1500	48.05418	0.31432	565.4182	7.36E+10	2E-05
1550	48.93856	0.31520	567.5588	6.45E+10	2.05E-05
1600	49.85369	0.31634	568.3984	5.51E+10	2.09E-05
1650	50.79218	0.31776	567.8002	4.54E+10	2.14E-05
1700	51.74659	0.31945	565.6271	3.55E+10	2.19E-05
1750	52.65256	0.32075	561.7422	2.53E+10	2.22E-05
1800	53.43097	0.32083	556.0084	1.47E+10	2.25E-05

Table 5.5: Thermo-mechanical properties of fifth layer from the top layer of FGM

Temperature (K)	Thermal conductivity (W/(m.K))	Poisson's ratio	Specific heat (J/(kg.K))	Modulus of elasticity (Pa)	Coefficient of thermal expansion (1/°C)
300	43.46225	0.31436	408.1348	2.07E+11	1.41E-05
500	33.10264	0.31816	433.2763	1.96E+11	1.6E-05
636	31.49895	0.32393	446.8052	1.86E+11	1.72E-05
700	31.29144	0.31436	454.323	1.8E+11	1.56E-05
750	32.52328	0.32753	455.1774	1.75E+11	1.8E-05
800	33.17868	0.33075	461.043	1.7E+11	1.85E-05
850	33.89301	0.33431	467.6212	1.64E+11	1.9E-05
900	34.97766	0.34248	474.7572	1.58E+11	1.97E-05
950	35.79314	0.34709	482.2957	1.52E+11	2.02E-05
1000	36.64001	0.35204	490.0817	1.45E+11	2.07E-05
1050	37.51064	0.35735	497.9602	1.38E+11	2.11E-05
1100	38.39741	0.36300	505.776	1.3E+11	2.16E-05
1150	39.2927	0.36900	513.3741	1.22E+11	2.21E-05
1200	40.18888	0.37535	520.5994	1.14E+11	2.25E-05
1250	41.07834	0.38205	527.2969	1.06E+11	2.3E-05
1300	41.95345	0.38910	533.3115	9.65E+10	2.35E-05
1350	42.80658	0.39649	538.4881	8.72E+10	2.39E-05
1400	38.79309	0.31436	542.6716	7.74E+10	1.82E-05
1450	39.39294	0.31479	545.7069	6.73E+10	1.87E-05
1500	40.05106	0.31556	547.4391	5.69E+10	1.92E-05
1550	40.75981	0.31669	547.713	4.6E+10	1.97E-05
1600	41.51157	0.31816	546.3736	3.48E+10	2.01E-05
1650	42.29873	0.31998	543.2657	2.32E+10	2.06E-05
1700	43.11366	0.32215	538.2343	1.13E+10	2.11E-05

Table 5.6: Thermo-mechanical properties of sixth layer from the top of FGM

Temperature (K)	Thermal conductivity (W/(m.K))	Poisson's ratio	Specific heat (J/(kg.K))	Modulus of elasticity (Pa)	Coefficient of thermal expansion (1/°C)
300	34.51387	0.31533	403.0536	2.07E+11	1.44E-05
500	27.16308	0.31997	417.3376	1.97E+11	1.64E-05
636	26.26264	0.32702	429.6508	1.86E+11	1.77E-05
700	25.82043	0.31533	437.2836	1.8E+11	1.55E-05
750	27.1527	0.33143	439.9959	1.75E+11	1.84E-05
800	27.75924	0.33536	446.5123	1.69E+11	1.89E-05
850	28.41814	0.33971	453.7001	1.63E+11	1.94E-05
900	29.51146	0.34970	461.3862	1.56E+11	2.02E-05
950	30.2591	0.35533	469.3975	1.49E+11	2.07E-05
1000	31.02988	0.36139	477.5608	1.41E+11	2.11E-05
1050	31.816	0.36787	485.7029	1.33E+11	2.16E-05
1100	32.60961	0.37478	493.6507	1.25E+11	2.21E-05
1150	33.40291	0.38212	501.2311	1.16E+11	2.26E-05
1200	34.18806	0.38988	508.2708	1.06E+11	2.3E-05
1250	34.95724	0.39806	514.5968	9.63E+10	2.35E-05
1300	35.70262	0.40667	520.0358	8.6E+10	2.4E-05
1350	36.41638	0.41571	524.4149	7.52E+10	2.45E-05
1400	31.17875	0.31533	527.5607	6.39E+10	1.74E-05
1450	31.57788	0.31585	529.3001	5.23E+10	1.79E-05
1500	32.04793	0.31680	529.46	4.01E+10	1.84E-05
1550	32.58106	0.31817	527.8673	2.76E+10	1.88E-05
1600	33.16946	0.31997	524.3487	1.45E+10	1.93E-05
1650	33.80529	0.32220	518.7312	1.05E+09	1.98E-05

Table 5.7: Thermo-mechanical properties of seventh layer from the top of FGM

Temperature (K)	Thermal conductivity (W/(m.K))	Poisson's ratio	Specific heat (J/(kg.K))	Modulus of elasticity (Pa)	Coefficient of thermal expansion (1/°C)
300	25.56549	0.31630	397.9725	2.07E+11	1.48E-05
500	21.22351	0.32179	401.399	1.98E+11	1.67E-05
636	21.02632	0.33012	412.4964	1.87E+11	1.81E-05
700	20.34943	0.31630	420.2443	1.8E+11	1.54E-05
750	21.78211	0.33533	424.8144	1.74E+11	1.88E-05
800	22.33981	0.33997	431.9816	1.68E+11	1.92E-05
850	22.94327	0.34512	439.779	1.61E+11	1.97E-05
900	24.04526	0.35692	448.0153	1.54E+11	2.06E-05
950	24.72505	0.36357	456.4993	1.46E+11	2.11E-05
1000	25.41975	0.37073	465.0399	1.37E+11	2.16E-05
1050	26.12135	0.37839	473.4456	1.28E+11	2.21E-05
1100	26.82182	0.38656	481.5254	1.19E+11	2.26E-05
1150	27.51312	0.39523	489.088	1.09E+11	2.31E-05
1200	28.18724	0.40440	495.9422	9.82E+10	2.35E-05
1250	28.83613	0.41407	501.8966	8.7E+10	2.4E-05
1300	29.45179	0.42425	506.7602	7.54E+10	2.45E-05
1350	30.02617	0.43493	510.3416	6.32E+10	2.5E-05
1400	23.56442	0.31630	512.4497	5.05E+10	1.66E-05
1450	23.76283	0.31691	512.8932	3.72E+10	1.71E-05
1500	24.0448	0.31804	511.4809	2.34E+10	1.75E-05
1550	24.40231	0.31966	508.0215	9.09E+09	1.8E-05

Table 5.8: Thermo-mechanical properties of bottom layer of FGM

Temperature (K)	Thermal conductivity (W/(m.K))	Poisson's ratio	Specific heat (J/(kg.K))	Modulus of elasticity (Pa)	Coefficient of thermal expansion (1/°C)
300	12.14291852	0.317756	390.3507	2.07788E+11	1.5321E-05
500	12.31415754	0.324512	377.4911	1.9915E+11	1.7315E-05
636	13.17185401	0.334766	386.7647	1.87274E+11	1.86709E-05
700	12.14291852	0.317756	394.6853	1.80004E+11	1.5321E-05
750	13.72623579	0.341177	402.0421	1.73575E+11	1.9309E-05
800	14.21065256	0.346891	410.1856	1.6649E+11	1.98075E-05
850	14.73096585	0.353225	418.8973	1.58748E+11	2.0306E-05
900	15.84595719	0.36775	427.9589	1.50349E+11	2.1303E-05
950	16.42397287	0.375942	437.1521	1.41293E+11	2.18015E-05
1000	17.0045603	0.384753	446.2585	1.31581E+11	2.23E-05
1050	17.5793883	0.394183	455.0597	1.21211E+11	2.27985E-05
1100	18.14012567	0.404233	463.3375	1.10185E+11	2.3297E-05
1150	18.67844123	0.414901	470.8734	98502262040	2.37955E-05
1200	19.18600378	0.426189	477.4492	86162527360	2.4294E-05
1250	19.65448215	0.438097	482.8464	73165995000	2.47925E-05
1300	20.07554514	0.450623	486.8467	59512664960	2.5291E-05
1350	20.44086155	0.463769	489.2318	45202537240	2.57896E-05
1400	12.14291852	0.317756	489.7833	30235611840	1.5321E-05
1450	12.04024044	0.318516	488.2829	14611888760	1.58195E-05

5.3. FGM Model Assumptions

In the present finite element model some assumptions are made as follows.

Laser hits on the top surface of the specimen perpendicularly and the nature of the beam is lower order Gaussian (TEM_{00}). The Gaussian distribution of the specimen is expressed by Eq. (5.4) [30],

$$q(x,y) = I_0 A exp(-\frac{x^2+y^2}{r^2}) \tag{5.4}$$

Where, I_0: beam intensity in watt/m^3, P: laser power in watt, A: co-efficient of absorption, r: radius of the beam in meter

a) Each layer of FGM material is isotropic and homogeneous in nature.
b) Diameter of the laser beam is 0.2 mm throughout the thickness of the specimen.
c) There is no effect of the assist gas such as gas pressure, cooling effect etc. and the effect of molten layer is negligible.
d) The bottom layer is Stainless steel (100%) and the top layer is Nickel(100%).
e) The temperature of atmosphere is 300 K.
f) The natural convection takes place due to the surrounding atmosphere and the convective heat transfer coefficient is 10 W/m^2K.
g) The top plane and the bottom plane are considered as a diffuse surface. Hence,the radiation heat transfer occurs and the emissivity is considered as 0.535.

5.4. Heat Transfer Analysis of FGM Model

From the Fourier's law, the 3D transient heat conduction mathematical model is represented by Eq. (5.5).

$$\rho c\left(\frac{\partial T}{\partial t}+V\frac{\partial T}{\partial t}\right)=\frac{\partial}{\partial x}\left(K\frac{\partial T}{\partial x}\right)+\frac{\partial}{\partial y}\left(K\frac{\partial T}{\partial y}\right)+\frac{\partial}{\partial z}\left(K\frac{\partial T}{\partial z}\right)+Q_G \tag{5.5}$$

Where, K: Thermal conductivity (W/m.K), c: Specific heat (J/kg.K), ρ : Density (kg/m^3), V: Velocity (m/s), Q_G: Rate of heat generation (W/m^3). Initial boundary condition of the specimen is shown by Eq. (5.6).

$$T(x,y,z,0) = T_0 \tag{5.6}$$

Where T_0: Ambient temperature (300 K). The free convection to atmosphere is considered as per Eq. (5.7) at bottom, top and lateral surfaces and the general boundary condition

$$Q_{convec} = h(T_s - T_0) \tag{5.7}$$

Where h: Convective heat transfer coefficient (W/m^2K), T_s: Surface temperature (^0C). The radiation heat loss is considered on the top and the bottom surface and the general boundary condition.

$$Q_{rad} = \epsilon \sigma A(T^4 - T_0^4) \tag{5.8}$$

Where ϵ : emissivity of the material, σ: Stefan–Boltzmann constant, A: Surface area.

The energy required for melting can be expressed by the Eq. (5.9).

$$E = \frac{\pi D^2}{4} \rho v t[C(T_M - T_0) + L] \tag{5.9}$$

Where, E: Energy required to melt (J), D: Diameter of laser beam (m), ρ: Density of the specimen (kg/m^3), υ: Penetration speed (m/s), t = Time(s), C: Specific heat (J/kg.K),T_M : Melting temperature (K), T_0: Ambient temperature (300 K), L: Latent heat of fusion (J/kg).

5.5. Thermal Stress Analysis of FGM Model

In the fusion cutting heat associated is concentrated in a very small region. When the laser beam is focused on a surface the temperature of the region is heated. Hence ,the surrounding surface gives compressive force on that region due to low temperature of the surrounding. Due to the temperature variation thermal stress is developed [62].

$$\sigma_{TH} = \frac{E\alpha\Delta T}{1 - v} \tag{5.10}$$

Where, E: Young's modulus, α : coefficient of thermal expansion, v: Poisson's ratio. The Von mises stress is given by the expression.

$$\sigma = \sqrt{\frac{(\sigma_1 - \sigma_2)^2 + (\sigma_2 - \sigma_3)^2(\sigma_1 - \sigma_3)^2}{2}} \tag{5.11}$$

Where $\sigma_1, \sigma_2, \sigma_3$ are the three principal stress along principal axis X, Y and Z axis respectively.

5.6. Meshing & Solutions

In this numerical simulation study, finite element software COMSOL MULTIPHYSICS 5.3a is used to simulate the thermo-mechanical model. The beam hits on the X-Z plane and travels along the X direction while the kerf is generated in the Z direction. The simulation is done on half of the specimen and used symmetry about X axis to minimize computational time. Dimension of the work piece is modeled as 15mm × 25mm × 8 mm (X × Y × Z). Each layer of FGM material is 1 mm thick and possesses the same material properties. Taking the same mesh, two different types of elements (coarse and fine) are considered in this simulation. In the mesh analysis, triangle type element is used on the top plane and 'Swift' option is used to copy the mesh in the whole specimen. Each layer consists of five distributions along the Y axis.

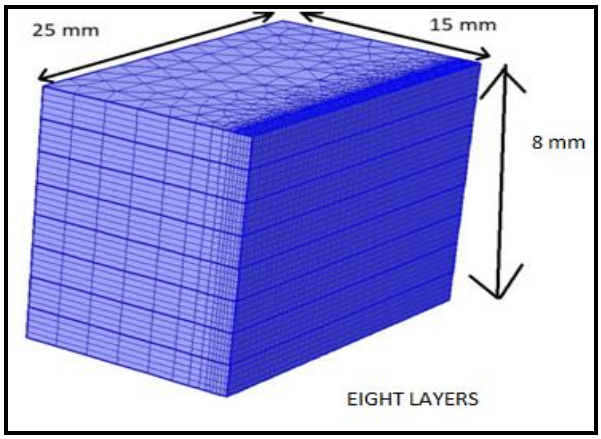

Fig 5.1: Dimensional details and meshed model of Ni-SS FGM rectangular block

The density of the mesh has a large effect on the result of the simulation model. High coarseness of mesh size leads to more erroneous results but needs less computational time. Whereas, the high fineness of mesh size provides more accurate results but needs more computational time. When the path is fine mesh, in that portion more accurate results are found even though computational time is more whereas the other part of specimen (ineffective part) which is coarse mesh decreases the computational time but can lead to less accurate results. In this nonlinear mesh model, total numbers of 73920 elements are considered. The travelling beam (heat flux) is simulated by varying the time steps. There is no element death methodology are considered in COMSOL MULTIPHYSICS 5.3a. Hence, by putting the value of young's modulus close to 0 and the Poisson ratio close to 0.5, the

elements which reach above the melting point are no longer take part any kind of interactions. From power law the thermal conductivity, specific heat, young's modulus, Poisson ratio, density and coefficient of thermal expansion of every layer are calculated.

5.7. Results and Discussion

In this FE simulation model study is developed to describe the fusion laser cutting of SS-Ni FGM material. This proposed model is the effect of process parameters in terms of laser power, scanning speed and beam radius on kerf width, depth of cut and thermal stress field are analyzed. The mesh structure of FE model shown in Fig. 5.1 is solved with the COMSOL MULTIPHYSICS version 5.3a.

a) Temperature Profile Analysis

The three dimensional temperature profile and the thermal stress data are extracted in the post processing stage. The temperature of a point along the cutting line varies at different time is shown in Fig. 5.2.

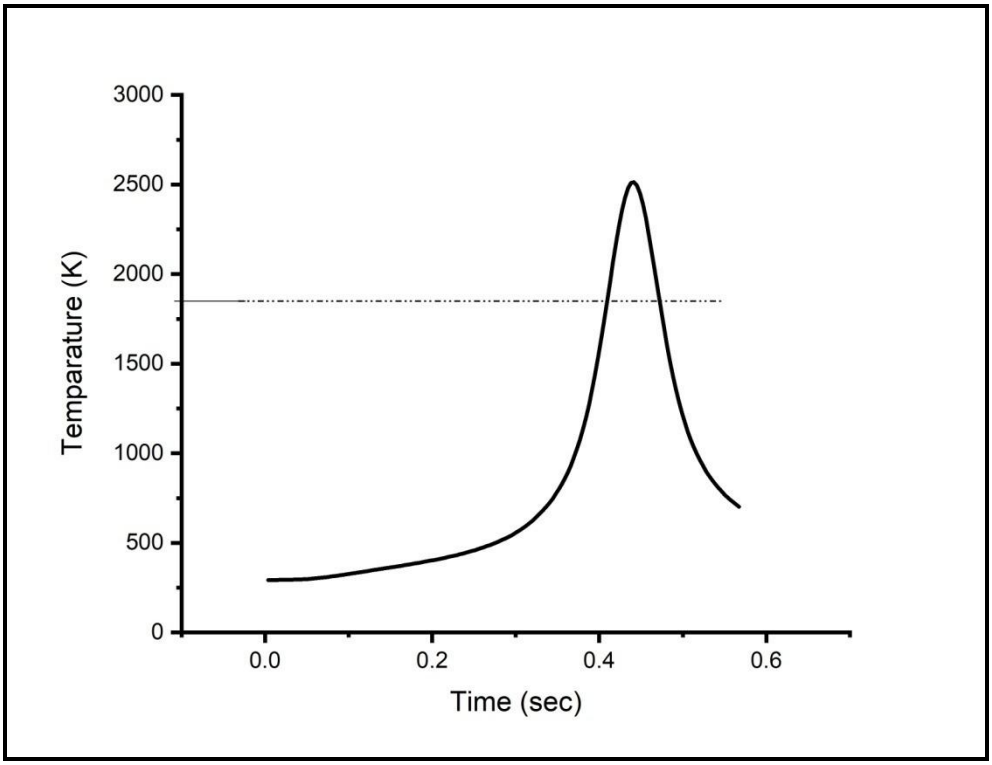

Fig 5.2: Temperature vs time

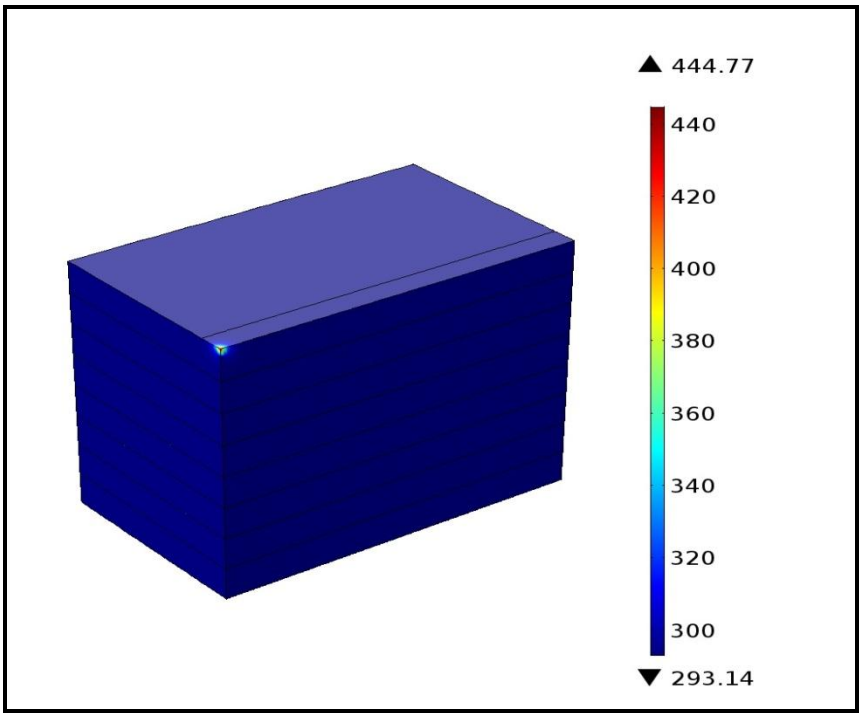
▲ 444.77
440
420
400
380
360
340
320
300
▼ 293.14

(a)

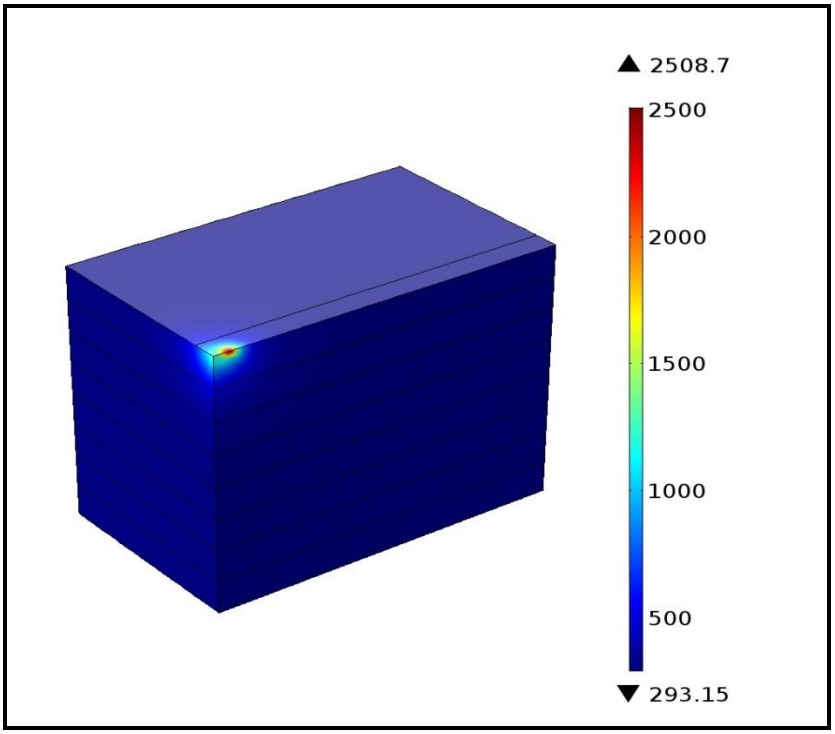
▲ 2508.7
2500
2000
1500
1000
500
▼ 293.15

(b)

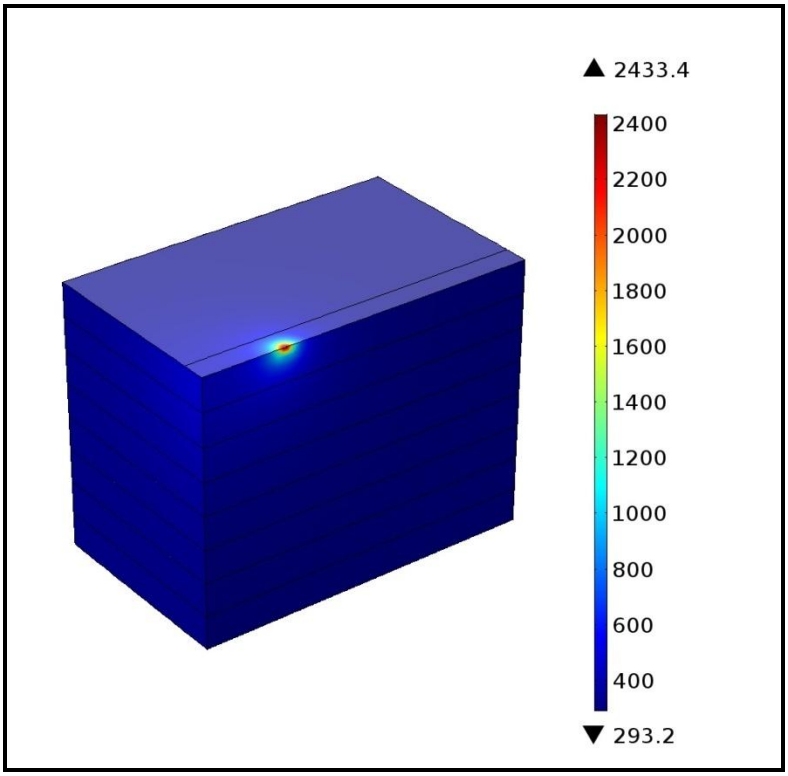

(c)

Fig 5.3: Temperature distribution across the Ni-SS FGM at different time

The three dimensional view of temperature profile and thermal stress of fusion laser cutting are shown in Fig. 5.3 and Fig. 5.4 respectively, while scanning speed is 5mm/sec. It is clearly observed from the Fig. 5.3 that the temperature along Y-axis decreases gradually with increase of distance from the laser beam along the thickness direction of the plate. The thermal stress in fusion cutting is created due to temperature gradient. In the FE model thermal stress is occurred at maximum laser power 200 Watt and scanning speed of 5mm/sec. While the laser beam incident on any point on the surface it gets heated but the other part is still at low temperature. As a result a compressive thermal stress is developed but when the beam passes the point of incident of laser beam a tensile stress is generated on that point shown in Fig. 5.4. Hence, FGM material is in advantageous position compare to the conventional materials.

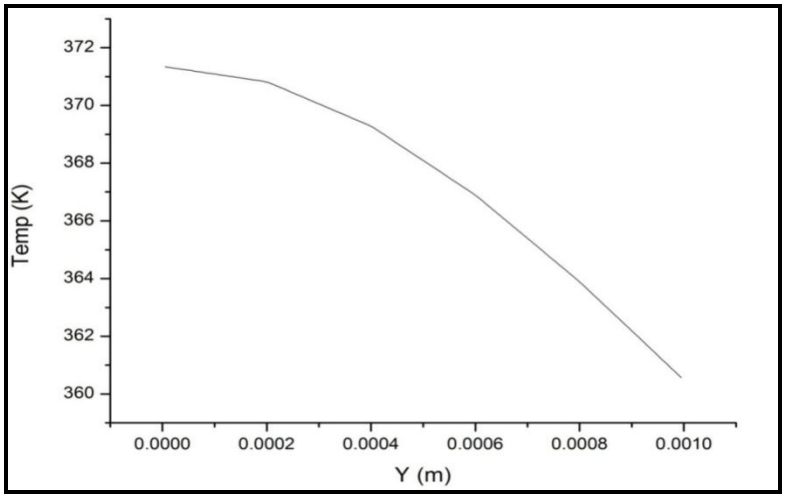

Fig. 5.4: Temperature vs. distance plot for laser machining of FGM at scanning speed :5mm/sec and laser power :200 Watt.

b) Stress Analysis

Fig. 5.5 predicts the stress intensity with varying time during the laser cutting of FGM materials. It can be observed from Fig. 5.5,the highest intensity is found time at 1 sec and the intensity is dying away from that time. Fig. 5.6 represents the von-misses stress vs time due to temperature variation at any point along the cutting line. When the laser beam is not on that point tensile stress is observed. On the other hand when the laser beam is on the point the compressive stress are generated on that point due to the temperature variation.

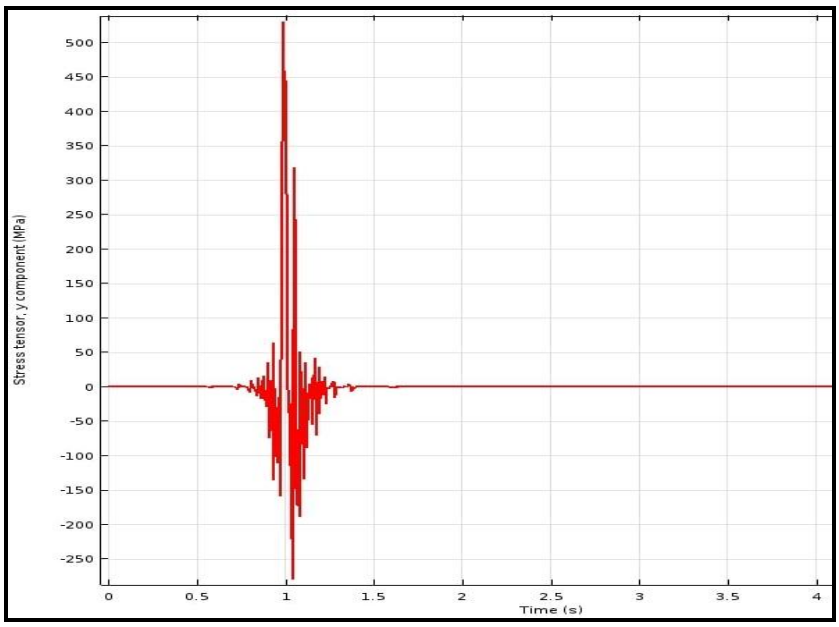

Fig. 5.5: Stress tensor vs. time plot of FGM laser machining for scanning speed (5mm/sec) and laser power (200 W).

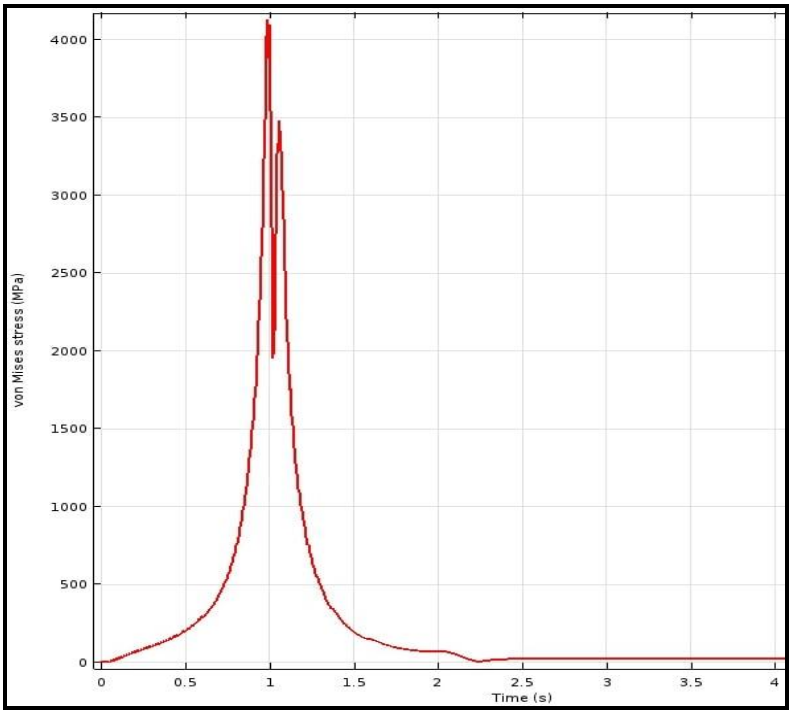

Fig. 5.6: Von mises stress vs. time plot of FGM laser machining for cutting speed (5mm/sec) and laser power (200 W).

c) Deformation Analysis

In the material due to temperature gradient and thermal stress deformation takes place which is shown in Fig. 5.7.

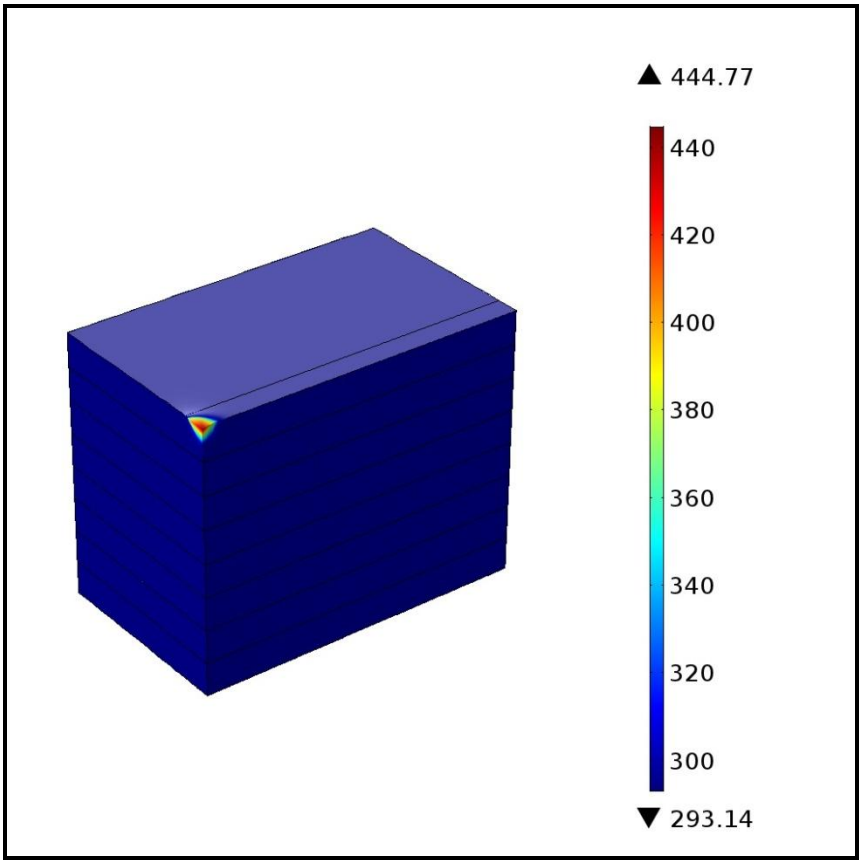

(a)

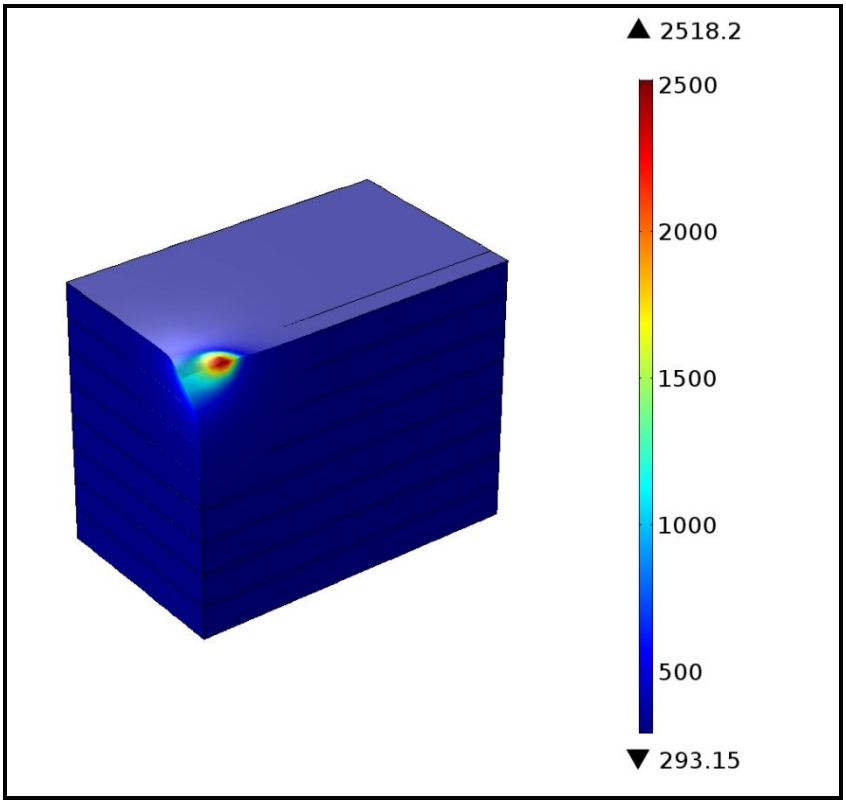

(b)

Fig 5.7: Deformation at time of FGM(Ni-SS) at different times

d) Kerf Width And Depth Analysis

Laser cutting is mainly dependent on the laser power, cutting speed and radius of the beam. Fig. 5.7 and 5.8 predicts the width and depth of the specimen at a constant cutting speed 5 mm/s and a constant beam radius 0.2 mm varying the power. When the power is more the specimen absorbs more heat. So the width and the depth of the material increase.

Table 5.9: Width of cut and Depth of cut of FGM from Numerical Simulation results at different Laser Power

SL No.	Laser Power (W)	Scanning Speed (mm/s)	Width (mm)	Depth (mm)
1	200	5	0.32	0.11
2	250	5	0.44	0.17
3	300	5	0.50	0.22
4	350	5	0.60	0.24
5	400	5	0.68	0.26
6	500	5	0.78	0.32
7	600	5	0.9	0.401
8	700	5	1.06	0.49
9	800	5	1.2	0.57
10	900	5	1.324	0.64
11	1000	5	1.33	0.65
12	1100	5	1.588	0.779
13	1200	5	1.722	0.9
14	1300	5	1.858	0.98
15	1400	5	1.91	1.07
16	1500	5	2.13	1.16
17	1600	5	2.35	1.26

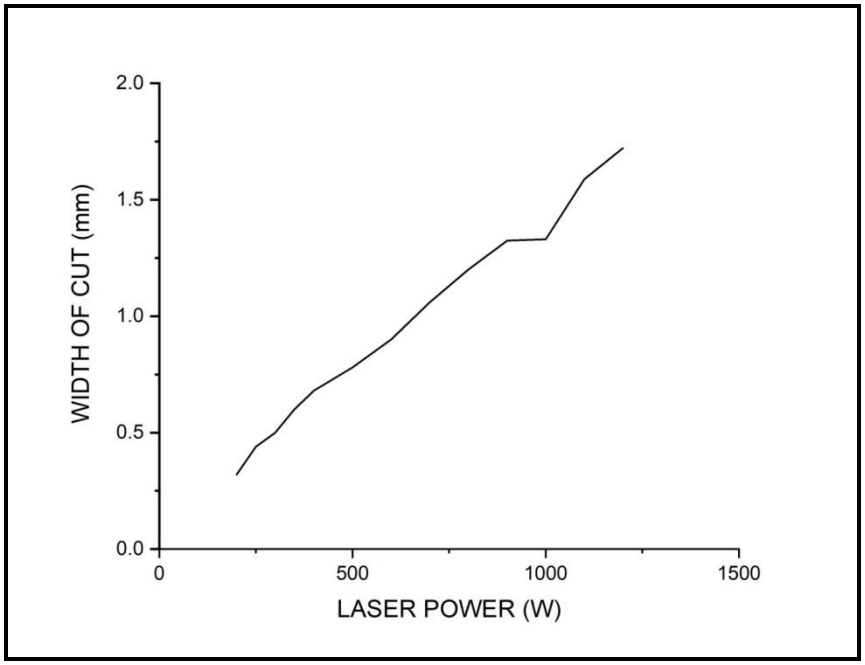

Fig. 5.7: Kerf width Vs Laser power plot of FGM laser machining for cutting speed (5mm/sec) and beam radius of 0.2mm

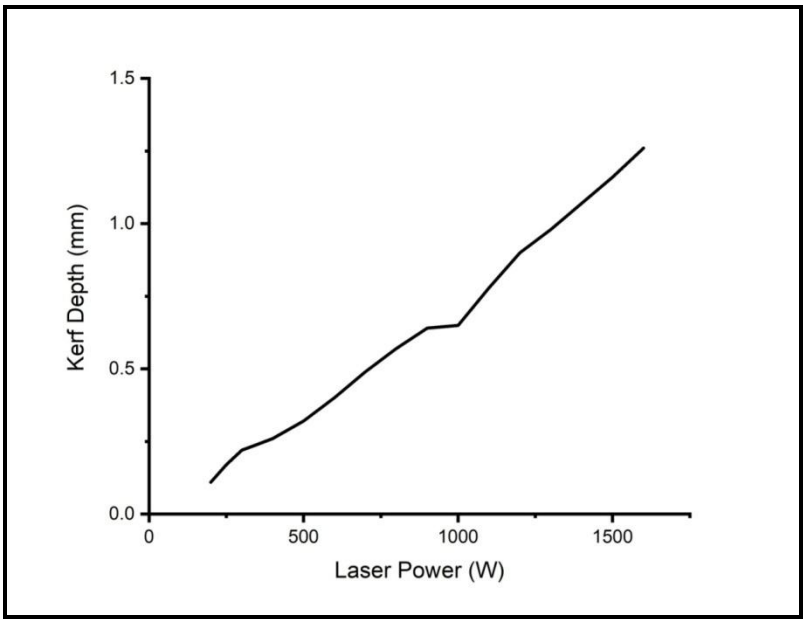

Fig. 5.8: Kerf depth vs Laser power plot of FGM laser machining for cutting speed (5mm/sec) and beam radius of 0.2 mm

Fig.5.9 and Fig 5.10 predict the width and depth of the specimen at a constant power of 400W and a constant beam radius of 0.2 mm with varying the scanning speed. When the

scanning speed is more, the specimen gets less time to absorb the heat. Therefore, with increasing the cutting speed width and depth decrease.

Table 5.10: Width of Cut and Depth of Cut of FGM from Numerical Simulation Results at Different Laser Scanning Speed

Sl. No.	Laser Power (W)	Scanning Speed (mm/s)	Width (mm)	Depth (mm)
1	400	2.5	0.86	0.32
2	400	5	0.68	0.26
3	400	7.5	0.64	0.26
4	400	10	0.62	0.25

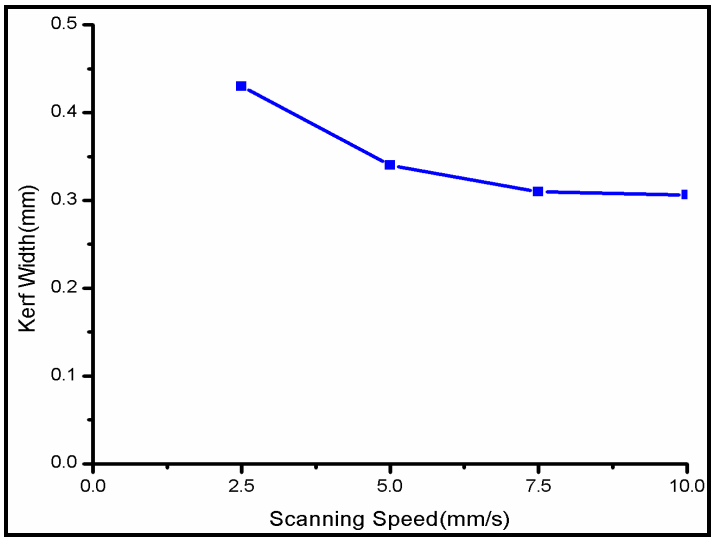

Fig. 5.9: Kerf width vs scanning speed plot of FGM laser machining for power 400W and beam radius of 0.2mm

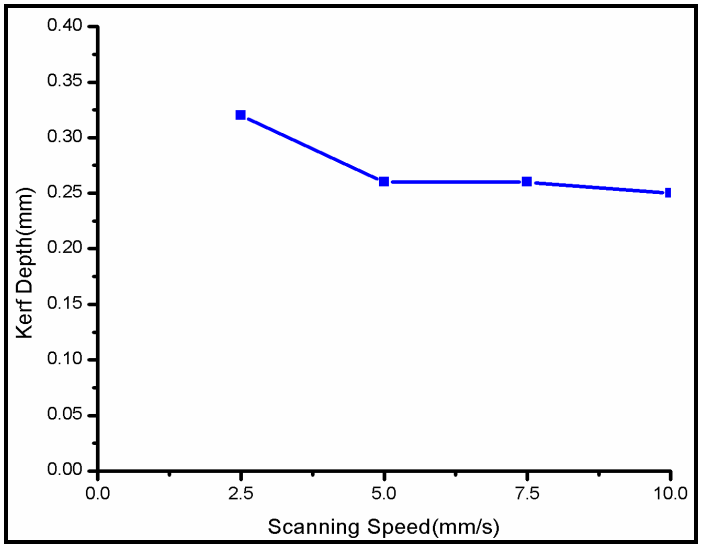

Fig. 5.10: Kerf depth vs scanning speed plot of FGM laser machining for power 400W and beam radius of 0.2mm

e) Young's modulus and Poisson ratio analysis

In simulation, young's modulus and poisson ratio analysis are done when young's modulus and poisson ratio values of any element reach near to 0 and 0.5 respectively then that element will be considered as dead element (element which does not interact with any heat) or removal element. Fig. 5.11(a) to Fig. 5.11(d) show material removal from the top layer of the FGM material.

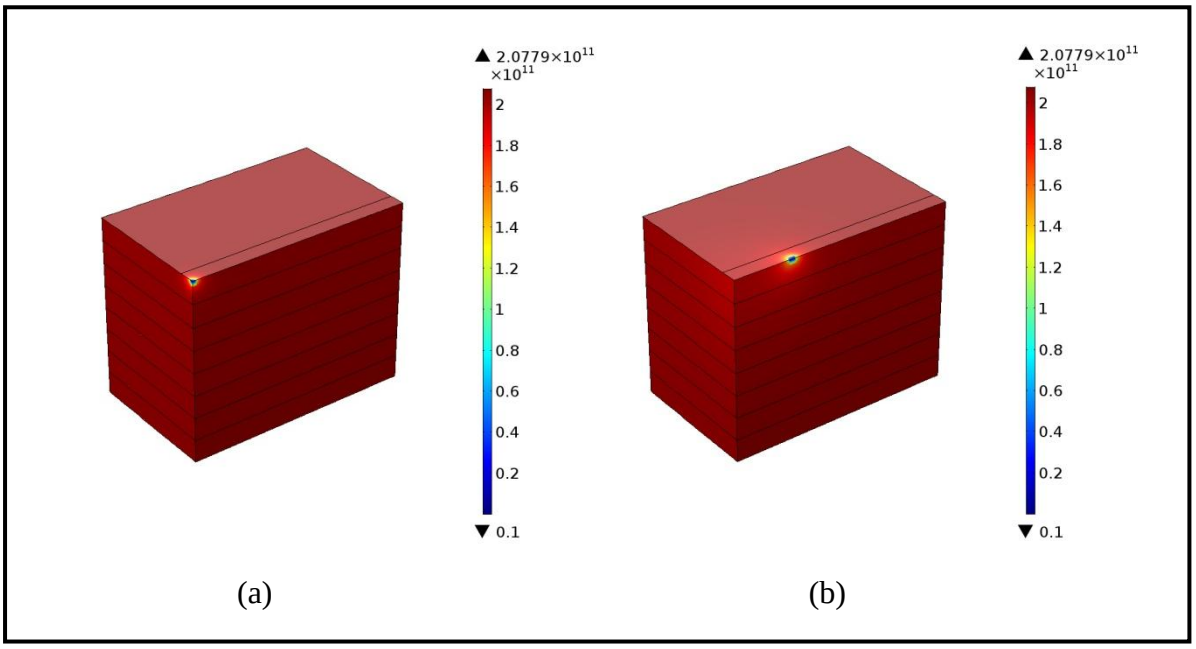

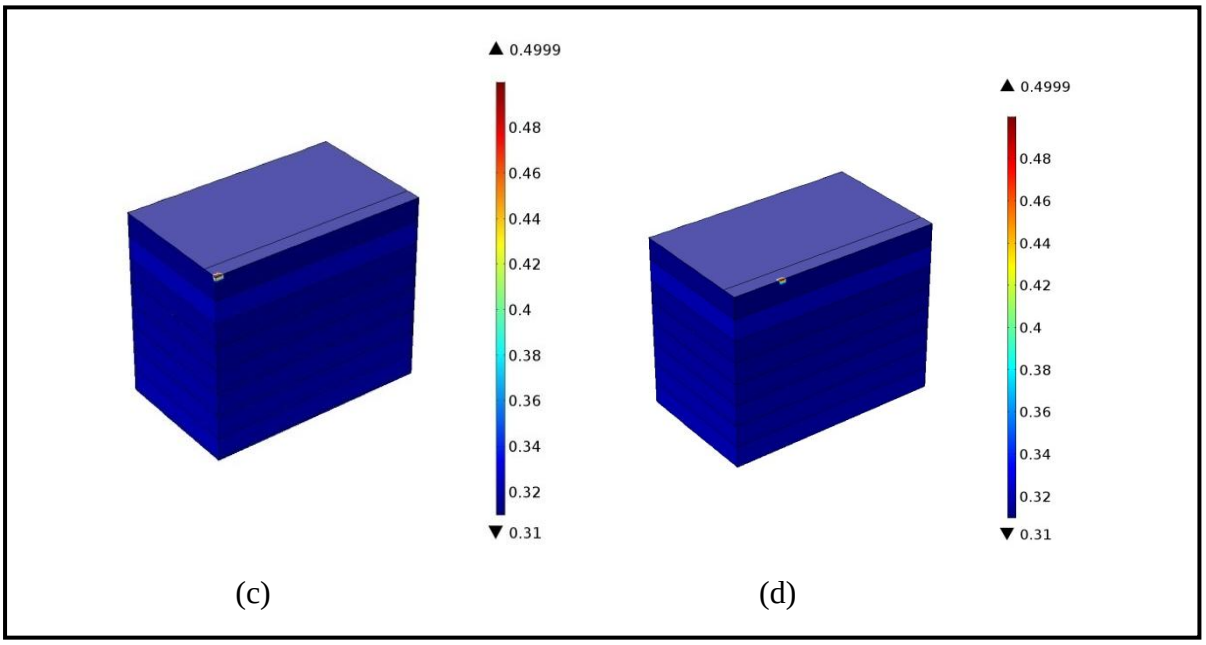

Fig. 5.11: (a) and (b) Young's modulus, (c)-(d) Poisson ratio

5.8. Conclusions

During this numerical simulation process of FGM laser machining a suitable methodology is established to determine the temperature gradient and stress distribution along the FGM material. This data will help the laser machining technique to evaluate the consecutive effects on the FGM material. From the present simulation results the following conclusions can be drawn.

a) A general procedure for simulation of laser cutting of FGM material is established. This procedure can be can be used for different powers and scanning speeds.
b) This simulated process will act as general guideline during experimental process of the laser cutting.
c) For the present simulation the temperature distribution along the thickness of the plate is determined numerically and it has been observed the temperature decreases drastically of the zone which is away of the laser machining zone along the direction of thickness of FGM material.
d) Highest stress intensity is found time at 1 sec and the intensity is dying down away from that time. For a given point compressive are observed when the laser beam is on the point

but tensile stress are found when the laser beam is away from that point due to the temperature variation.

e) The width and depth increase with the increase of laser power but decrease with the increase of the scanning speed.

Chapter 6: Overall Conclusions and Future Scope

6.1. Overall Conclusions

A transient thermo-mechanical analysis of laser cutting on Functionally Graded Material (FGM) is carried out using verified with laser cutting of stainless steel(experimental and simulation) to obtain the thermal stress, displacement, kerf width and depth of cut in the plate and thereby to understand the mechanism of laser cutting process with greater insight. The The work carried out in the present thesis can be summarised as follows.

a) Summary of laser cutting on Stainless steel (AISI-304)

Laser cutting of 0.5 mm thick stainless steel AISI-304 sheet was performed by using finite element numerical analysis to predict kerf width and depth of cut. The results of numerical mathematical model were validated by experiment results. Comsol multiphysics 5.3a was used to simulate the lower order Gaussian heat source and putting Young's modulus tends to zero and Poisson ratio 0.5 element death methodology was employed for material removal. The proposed thermo-mechanical simulation was a combination of heat transfer and solid mechanics (mechanical) analysis. The simulation results of heat transfer analyses how that the kerf width increases with an increase in laser power and decreases with an increase in scanning speed. Moreover the temperature rises sharply near the focused laser beam. However, temperature gradient decreases gradually and sharply with the increase of distance from the cutting edge. From the solid mechanics analysis the results of thermal stress was identified. It was found that maximum stress concentrations were observed at the cutting edge especially at the middle of the specimen which was supported by the analysis of optical microscope.

b) Summary of laser cutting on FGM

i. A general procedure for simulation of laser cutting of FGM material is established. This procedure can be can be used for different powers and scanning speeds.
ii. This simulated process will act as general guideline during experimental process of the laser cutting.
iii. For the present simulation the temperature distribution along the thickness of the plate is determined numerically and it has been observed the temperature decreases drastically of the zone which is away of the laser machining zone along the direction of thickness of FGM material.
iv. Highest stress intensity is found time at 1 sec and the intensity is dying down away from that time. For a given point compressive are observed when the laser beam is on the point but tensile stress are found when the laser beam is away from that point due to the temperature variation.
v. The width and depth increase with the increase of laser power but decrease with the increase of the scanning speed.
vi. After penetrating the first layer due to change in properties of the material, the slope of depth of cut vs power is slightly changed.

6.2. Future scope

The future scopes of the present work are given below.

i. Further experimental investigation of laser cutting of functionally graded material can be performed to validate the numerical simulation results already performed.
ii. Frequency, laser beam mode and stand of distance can be considered as input process parameter in future study.
iii. Role of the molten fluid pressure and assist gas pressure can be treated as input process parameters to carry out further research work.
iv. The volume fraction can be varied for modelling the functionally graded material in the further numerical study.
v. The optimum cutting speed for a particular material can be perform by obtaining minimum Heat Affected Zone and distortion using different modes like continuous mode laser, pulsed mode laser etc.

vi. Variety of materials like another types of Functional graded material, shape memory alloy, and composite materials can be considered for experimental and numerical investigations .

References

1. Csele M. Fundamental of Light Sources and Lasers A John Wiley & Sons, Inc., Publication; 2004.
2. Reddy J N. Mechanics of laminated composite plates and shells: theory and analysis. CRC Press; 2004.
3. Ion J. Laser processing of engineering materials: principles, procedure and industrial application. Elsevier; 2005.
4. Shanmugam N.S. , Buvanashekaran G, Sankaranarayanasamy K, Manonmani K. Some studies on temperature profiles in AISI 304 stainless steel sheet during laser beam welding using FE simulation. The International Journal of Advanced Manufacturing Technology. 2009; 43: 78.
5. Sheng PS, Joshi VS. Analysis of Heat-Affected Zone Formation for Laser Cutting of Stainless-Steel. Journal of Materials Processing Technology. 1995; 53: 879
6. Masumoto I, Shinoda T, Hirate T. Weld Decay Recovery by Laser Beam Surfacing of Austenitic Stainless Steel Welded Joints. Transactions of the Japan Welding Society. 1990; 21: 11.
7. Jamshidi Aval H., Farzadi A., Serajzadeh S., Kokabi A.H. Theoretical and experimental study of microstructures and weld pool geometry during GTAW of 304 stainless steel. The International Journal of Advanced Manufacturing Technology. 2009; 42: 1043.
8. Hassan E.H. Advance machining process. DOI: 10.1036/0071466940. page 9
9. https://www.nmri.go.jp/oldpages/eng/khirata/metalwork/milling/drill/index_e.html
10. https://images.app.goo.gl/K2a76iJLHKMVuQqX8
11. https://images.app.goo.gl/4fMHSQ6CQT94AAv16
12. https://www.indiamart.com/proddetail/all-geared-shaping-machine-4463084497.html
13. https://nptel.ac.in/courses/112105127/pdf/LM-37.pdf
14. https://images.app.goo.gl/h8L5fU1yk4dQ1XD16
15. https://www.mechanicalbooster.com/2017/05/water-jet-machining.html
16. https://nptel.ac.in/courses/112105127/pdf/LM-36.pdf
17. https://images.app.goo.gl/MMu6MRSjBoZbXCMt7
18. https://images.app.goo.gl/LM7h3zUgH1pBjuga8

19. Negarestani R. Laser cutting of carbon fibre-reinforced polymercomposite materials, PhD thesis. School of Mechanical, Aerospace and Civil Engineering. The University of Manchester. 2010
20. Balasubramaniuam K.R,Siva shanmugam, N.,Buvanshekaran G.,Sankaranarayanasamy K. Numerical and experimental investigation of laser beam welding of AISI 304 stainless steel. ARPN Journal of Engineering and Applied Sciences.2018; 3: 93.
21. https://www.lenntech.com/stainless-steel-304.htm
22. https://www.jessytrade.com/home/laser-cut-stainless-steel-profiles/
23. Mahamood R.M. and Akinlabi E.T. Functionally Graded Materials .Springer International Publishing AG 2017 . DOI 10.1007/978-3-319-53756-6_2
24. https://images.app.goo.gl/vfHG9zFNS394YgQUA
25. Wandera C., Salminen A., Olsen F.O. and Kujanpää V. Cutting of stainless steel with fiber and disk laser. Citation: ICALEO 2006; 404.
26. Wandera C. and Kujanpää V. Optimization of parameters for fibre laser cutting of a 10 mm stainless steel plate. Proc. IMechE Engineering Manufacture. 225.
27. Stelzera S., Mahrlea A., Wetziga A., Beyera E. Experimental investigations on fusion cutting stainless steel with fiber and CO2 laser beams, , Physics Procedia. 2013; 41: 399.
28. Wandera, Salminen, and Kujanpaa . Optimization of parameters for fibre laser cutting of a 10 mm stainless steel plate, J. Laser Appl.2009; 21
29. Nyon K. Y., Nyeoh C. Y., Mokhtar M. and Rahman R. A. Finite element analysis of laser inert gas cutting on Inconel 718 , Int J Adv Manuf Technol 2012; 60:995.
30. Sifullah A. M., Nukman Y., Hassan M. A. and Hossain A. Finite element analysis of fusion laser cutting on stainless steel-304. 2016; 11: 1819.
31. Fu C.H., Liu J.F., Guo A. Statistical characteristics of surface integrity by fiber laser cutting of Nitinol vascular stents, Applied Surface Science 2015; 353: 291.
32. Kardas O. O., Keles O., Akhtar S., Yilbas B. S., Laser cutting of rectangular geometry in 2024 aluminum alloy: Thermal stress analysis, Optics & Laser Technology 2014; 64: 247.
33. Wang J. An experimental analysis and optimisation of the CO_2 laser cutting process for metallic coated sheet steels. The International Journal of Advanced Manufacturing Technology. 2000; 16: 334.

34. Rotter JM. Shell structures: the new European standard and current research needs. Thin-walled structures. 1998; 31: 3.
35. Meirovitch L. Principles and techniques of vibrations. New Jersey: Prentice Hall; 1997.
36. Rao JS. Turbomachine blade vibration. New Age International; 1991.
37. Birman V, Byrd LW. Modeling and analysis of functionally graded materials and structures. Applied mechanics reviews. 2007; 60: 195.
38. Liew KM, Zhao X, Ferreira AJ. A review of meshless methods for laminated and functionally graded plates and shells. Composite Structures. 2011; 93: 2031.
39. Alijani F, Amabili M. Non-linear vibrations of shells: A literature review from 2003 to 2013. International Journal of Non-Linear Mechanics. 2014; 58: 233.
40. Jha DK, Kant T, Singh RK. A critical review of recent research on functionally graded plates. Composite Structures. 2013; 96: 833.
41. Thai HT, Kim SE. A review of theories for the modeling and analysis of functionally graded plates and shells. Composite Structures. 2015; 128: 70.
42. Swaminathan K, Naveenkumar DT, Zenkour AM, Carrera E. Stress, vibration and buckling analyses of FGM plates—a state-of-the-art review. Composite Structures. 2015; 120: 10.
43. Gupta A, Talha M. Recent development in modeling and analysis of functionally graded materials and structures. Progress in Aerospace Sciences. 2015; 79: 1.
44. Liew KM, Lei ZX, Zhang LW. Mechanical analysis of functionally graded carbon nanotube reinforced composites: a review. Composite Structures. 2015; 120: 90.
45. Swaminathan K, Sangeetha DM. Thermal analysis of FGM plates–A critical review of various modeling techniques and solution methods. Composite Structures. 2017; 160: 43.
46. Zhao X, Liew KM. Free vibration analysis of functionally graded conical shell panels by a meshless method. Composite Structures. 2011a; 93: 649.
47. Tornabene F, Fantuzzi N, Bacciocchi M. Free vibrations of free-form doubly-curved shells made of functionally graded materials using higher-order equivalent single layer theories. Composites Part B: Engineering. 2014; 67: 490.
48. https://en.wikipedia.org/wiki/COMSOL_Multiphysics
49. https://www.comsol.com/blogs/what-is-comsol-multiphysics/

50. Yusoff N, Ismail SR, Mamat A, Ahmad-Yazid A. Selected Malaysian Wood CO2-Laser Cutting Parameters and Cut Quality. American Journal of Applied Sciences. 2008; 5 : 990.
51. Chen S-L. The effects of high-pressure assistant-gas flow on high-power CO_2 laser cutting. Journal of Materials Processing Technology. 1999; 88: 57.
52. Reddy J. N. and Chin C. D. Thermomechanical analysis of functionally graded cylinders and plates , ISSN: 0149-5739.
53. Steen W. M., Mazumder J., Watkins K. G., Laser material processing. Springer. 2003.
54. Boyden S, Zhang Y. Temperature and wavelength-dependent spectral absorptivities of metallic materials in the infrared. Journal of thermophysics and heat transfer. 2006; 20: 9.
55. Mazumder J, Steen W. Heat transfer model for CW laser material processing. Journal of Applied Physics 1980; 51: 941.
56. YCC C. W. T., Leung, Bernard N.W., Tsun, John, C.K. Alex. Characterization of Kovar-to-Kovar laser welded joints and its mechanical strength. Optics and Lasers in. 2005.
57. Engineering. 43:151.
58. Khan O. U., Yilbas B. Laser heating of sheet metal and thermal stress development. Journal of materials processing technology. 2004; 155: 2045.
59. Lanhe W. Thermal buckling of a simply supported moderately thick rectangular FGM plate , Composite Structures 2004; 64: 211.
60. Das A, Karmakar A. Free Vibration Characteristics of Functionally Graded Pre-twisted Conical Shells under Rotation. Journal of The Institution of Engineers (India): Series C. 2017: 1.
61. Das A, Sarkar S, Karmakar A. Vibration Characteristics of Functionally Graded Pre-Twisted Turbo Machinery Blade with Rotational Effect. Advanced Science Letters. 2016; 22: 111.
62. Nasab H. M., Golabi S. FEM Simulation of the Bending Angle During the Laser Forming of FGM Plates. Journal of Thermal Stresses. 2015; 38: 1034.